Journal of Neuroinflammation

RESEARCH

Open Access

Tet1-mediated 5hmC regulates hippocampal neuroinflammation via wnt signaling as a novel mechanism in obstructive sleep apnoea leads to cognitive deficit

Yaru Kong[1,2,3†], Jie Ji[4†], Xiaojun Zhan[3†], Weiheng Yan[1,2,3], Fan Liu[1,2,5], Pengfei Ye[3], Shan Wang[5*] and Jun Tai[1,3*]

Abstract

Background Obstructive sleep apnoea (OSA) is a sleep-disordered breathing characterized by intermittent hypoxia (IH) that may cause cognitive dysfunction. However, the impact of IH on molecular processes involved in cognitive function remains unclear.

Methods C57BL / 6 J mice were exposed to either normoxia (control) or IH for 6 weeks. DNA hydroxymethylation was quantified by hydroxymethylated DNA immunoprecipitation (hMeDIP) sequencing. ten-eleven translocation 1 (*Tet1)* was knocked down by lentivirus. Specifically, cognitive function was assessed by behavioral experiments, pathological features were assessed by HE staining, the hippocampal DNA hydroxymethylation was examined by DNA dot blot and immunohistochemical staining, while the Wnt signaling pathway and its downstream effects were studied using qRT-PCR, immunofluorescence staining, and Luminex liquid suspension chip analysis.

Results IH mice showed pathological changes and cognitive dysfunction in the hippocampus. Compared with the control group, IH mice exhibited global DNA hydroxylmethylation in the hippocampus, and the expression of three hydroxylmethylases increased significantly. The Wnt signaling pathway was activated, and the mRNA and 5hmC levels of *Wnt3a*, *Ccnd2*, and *Prickle2* were significantly up-regulated. Further caused downstream neurogenesis abnormalities and neuroinflammatory activation, manifested as increased expression of IBA1 (a marker of microglia), GFAP (a marker of astrocytes), and DCX (a marker of immature neurons), as well as a range of inflammatory cytokines (e.g. TNFa, IL3, IL9, and IL17A). After *Tet1* knocked down, the above indicators return to normal.

Conclusion Activation of Wnt signaling pathway by hippocampal *Tet1* is associated with cognitive dysfunction induced by IH.

Keywords $5hmC_1$, IH_2, $Tet1_3$, Wnt $pathway_4$, $hippocampus_5$

†Yaru Kong, Jie Ji and Xiaojun Zhan contributed equally to this work.

*Correspondence:
Shan Wang
wsaquarius@sina.com
Jun Tai
trenttj@163.com

Full list of author information is available at the end of the article

Graphical Abstract

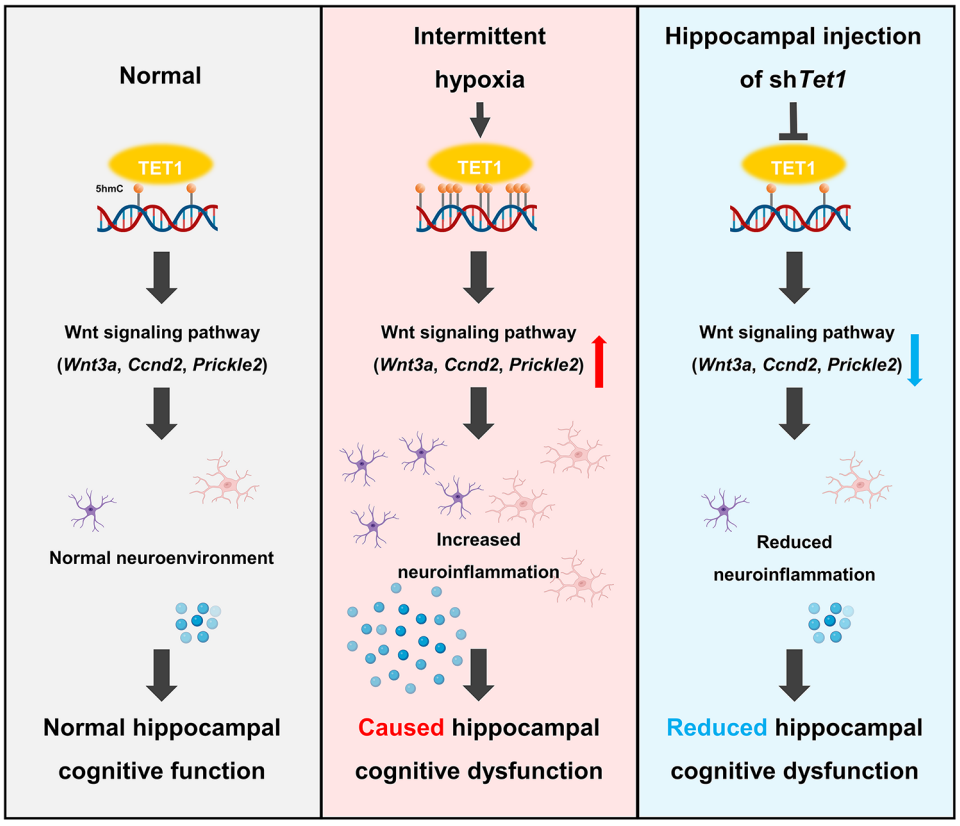

Introduction

Obstructive sleep apnoea (OSA) is the most common type of sleep-disordered breathing, affecting approximately 1 billion adults worldwide; the largest number of OSA in China [1]. OSA is characterized by recurrent upper airway obstruction during sleep, resulting in intermittent hypoxia (IH), sleep fragmentation, further systemic inflammation and oxidative stress [2]. Untreated OSA is widely recognized to be associated with an increased risk of hypertension [3], diabetes [4], and cognitive dysfunction [5], leading to substantial health and social burdens. In particular, the consequences of cognitive dysfunction, which includes impaired neurodevelopment in children [6, 7] and neurodegenerative diseases in elderly individuals [8], have received extensive attention in recent years. Cognitive dysfunction in OSA patients may be related to regional hippocampal volume changes; an increase in the volume suggests inflammation and glial activation and a decrease in volume may be a result of long-term neuronal damage [9]. IH may play a central role in causing attention, memory and executive function impairment in OSA patients [10]. In vivo experiments have demonstrated that IH can drive cognitive dysfunction through microglia-mediated hippocampal inflammatory injury in mice [11]. However, the specific molecular mechanism involved is unclear.

DNA methylation, one of the most studied epigenetic modifications, occurs at the 5-carbon position of cytosine residues to generate 5-methylcytosine (5mC), which was once considered to be stable [12]. The ten-eleven translocation (TET) enzymes TET1-3 are members of the 2-oxoglutarate-dependent dioxygenase (2-OGDD) family and oxidize DNA 5mC to 5-hydroxymethylcytosine (5hmC), suggesting a novel mechanism for DNA demethylation [13, 14]. While the levels of 5mC are comparable across organs throughout the body, the distribution of 5hmC varies depending on tissue or cell type, with particularly high levels in mature neurons in the central nervous system (CNS) [15]. Given that 5hmC levels were found to increase progressively from early postnatal to adulthood in the cerebellum and hippocampus of mice, it is suggested that 5hmC may play a directly involved in neurodevelopment and aging [16]. More importantly, 5hmC levels were significantly increased in the brain of Alzheimer's disease patients, indicating that the changes of 5hmC are not only age-dependent, but may be suggestive of neurodegeneration and disease [17]. Furthermore, TETs mediated DNA hydroxymethylation may be

involved in regulating neuronal activity and cognitive processes [18–21]. TET1 has been found to be the most characterized member of the TET family involved in learning and memory; however, this phenomenon is also controversial [22]. Both the loss and overexpression of *Tet1* have been reported to enhance or impair memory, which may be related to the cell type specificity of TET1 [18, 23–27]. For instance, knockdown of *Tet1* specifically in hippocampal astrocytes not only significantly reduced global 5hmC levels, but also resulted in abnormal neuronal development and impaired cognitive function [24]. However, *Tet1* overexpression in hippocampal CA1 pyramidal cells contributed to long-term memory impairment after episodic fear conditioning, through strong raised 5hmC levels [25]. Although it is well established that TETs requires oxygen for catalytic activity, the data reported on the response of TETs to hypoxia are conflicting. In a variety of tumour cells, hypoxia can directly reduce the oxidative activity of TETs to promote DNA demethylation, while total TETs expression is unchanged [28, 29]. However, hypoxia increases *TET1* expression and 5hmC levels in certain types of cells, such as neuroblastoma [28, 30] and glioblastoma cells [31], probably because *Tet1* coactivates with hypoxia-inducible factor independently of enzymatic activity [30, 32, 33]. In addition, TET1 also links cellular redox status and epigenome maintenance, which mediates the increased 5hmC formation under oxidative stress [34]. Therefore, TETs and 5hmC changes in hippocampal cognitive dysfunction induced by IH, a specific chronic mild hypoxia, deserve to be investigated.

The Wnt signaling pathway is the most important cascade in the nervous system, which is divided into the canonical β-catenin pathway, as well as the atypical Ca^{+} and planar cell polarity (PCP) pathways, coordinating synaptic function, adult neurogenesis, and neuroimmune interactions in the brain [35–37]. Its dysregulation participates in neuroinflammation and neurogenesis, causing cognitive dysfunction in a variety of neurodegenerative and neuropsychiatric diseases [38, 39]. In ApoE-KO AD organoids, aberrant Wnt pathway activation leads to abnormal neurogenesis, including decreased excitatory neurons and increased glial and inhibitory neurons [40]. Abnormal activation of Wnt pathway was also found in the hippocampus of LPS-induced depression mice, with decreased mature neurons and activation of glial cells, leading to cognitive decline [41]. In addition, activation of the Wnt pathway was found in OSA patients with hypertension and IH-treated cardiomyocytes [42, 43]. Therefore, we hypothesized that the Wnt pathway plays an important role in IH-mediated hippocampal cognitive dysfunction in mice.

Here, we assessed the role of DNA demethylation in cognitive dysfunction in IH mice. In addition, the therapeutic effect of hippocampal-specific knockdown of *Tet1* was investigated. This study aims to reveal the neuroinflammation -related molecular regulatory mechanism of OSA with cognitive dysfunction from the perspective of Wnt signaling activation in the hippocampus.

Materials and methods

Animals

8-week-old male BALB/c mice, weighing 18–20 g, were purchased from Beijing Shenghe Experimental Animal Technology Co., Ltd. The mice were kept at a specific pathogen-free condition of 18–26 ℃ and 40–70% humidity, accompanied by a standard light-dark cycle. Experiments were performed in strict accordance with institutional ethical codes and were approved by the Animal Care and Use Ethics Committee of the Capital Institute of Pediatrics (DWLL2021016).

Cell culture and transfection

Human embryonic kidney cell line 293T and mouse brain neuroma cell line N2A were obtained from the Capital Institute of Pediatrics Cell Bank. The cells were cultured in Dulbecco's modified Eagle's medium (DMEM; Gibco, USA) with 10% fetal bovine serum (FBS; Gibco), 100 μg/mL penicillin and 100 μg/mL streptomycin (Gibco) at 37 °C and 5% CO_2. To interfere the expression of *Tet1*, a shRNA interference sequence targeting *Tet1* (5'-3': GC AATCAGTTAGCAGACTTGA) was designed and synthesized and named *shTet1*. The negative control virus was named shNC. These are purchased from Genechem (Shanghai, China). 293Ts were used for infections with a MOI of 1. N2As were used for infections with a MOI of 20. 72 h after transfection, the relative amount of green fluorescence in 293Ts was observed under a high-content microscope (Theo Fisher, USA), and N2As were collected for PCR identification.

Group, modeling and treatment

Group

Acclimatization to the new environment for 3 days. Mice were randomly divided into 4 groups: control group, IH group, IH+shNC group and IH+shTet1 group. In order to prevent any interference between experiments, certain mice were exclusively monitored for hippocampal oxygen partial pressure (PO2), functional magnetic resonance imaging (fMRI) parameters, or behavioral tests. The remaining mice had their hippocampal tissues utilized for molecular biology experiments.

Modeling

IH group, IH+shNC group, and IH+sh*Tet1* group were exposed to IH for 6 weeks using a hyperbaric oxygen chamber (Beijing Zhongshi Dichuang Technology Development Co., Ltd., China). The IH mode was 1 min

alternating cycle (oxygen concentration 5-21%) for 8 h / d (8:00 am to 4:00 pm) [44]. The control group was maintained in room air. At the end of the 4th week of IH, body weight (n=20/ group) was measured in the control and IH groups, and a part of mice were euthanized after hippocampal PO_2 (n=6/ group) and fMRI parameters (n=6/ group) were measured.

Treatment

In order to interfere the expression of *Tet1*, lentiviral shRNA interference sequences targeting *Tet1* were designed, synthesized and named sh*Tet1*. The negative control viruses were named shNC. After 4 weeks of IH treatment, IH+shNC and IH+sh*Tet1* mice were injected with shNC and sh*Tet1* in the hippocampus, respectively. In brief, mice were anesthetized with isoflurane and fixed in the stereotaxy (Beijing Zhongshi Dichuang Technology Development Co., Ltd.). Artificial tear ointment was applied to the eyes of the mice. Hair was cut off from the top of the skull and a longitudinal incision was made in the skin. Blunt dissection was used to remove connective tissue overlying the skull. Two holes were made in the skull using a small dental drill, with coordinates of ±1.9 mm inter-aural, − 1.4 mm relative to the bregma, and +1.8 mm from the dural surface [45]. The injection infusion rate was set at 0.8 μL/min, and the total infusion volume was 1μL/hemisphere. After infusion, the needle was left in place for 1 min to minimize diffusion and then slowly withdrawn. Finally, the incision was sutured and the mice were returned to their cages.

At the end of the 6th week of IH, a part of mice in each group were assessed for behavior and euthanized, and the brains of the remaining mice were quickly removed and processed for study after euthanasia.

Hippocampal PO_2

The PO_2 value in the hippocampus of mice was detected by tissue oxygen partial pressure detection device (Beijing Zhongshi Dichuang Technology Development Co., Ltd.). In brief, a stereotaxy was used to fix isoflurane-anesthetized mice and guide the probe into the hippocampus. PO_2 was detected in real time. It was recorded until PO_2 values were in the 10% range for 3 min. The left and right hippocampi were averaged.

fMRI data acquisition and analysis

The MRI scanning was performed by the BRUKER 7.0-T MRI (Bruker Pharmasca 7.0/16us, Germany) scanner. Anatomical images were acquired using rapid acquisition with relaxation enhancement (RARE) sequence with the following parameters: matrix size 256×256, field of view (FOV)=2 cm × 2 cm, repetition time (TR)/ echo time (TE)=4500/45 ms, and number of excitation (NEX)=4. Functional scans were acquired using gradient-echo planar imaging (EPI): slice thickness=1 mm, matrix size=80×64, FOV=2.43 cm x 2.1 cm, TR/TE=2000/15 ms, and NEX=1. Statistical parametric mapping software was used for image pre-processing and statistical analysis. The blood oxygenation level dependent (BOLD) values were analyzed and compared between the the control and IH groups. All functional image post-processing was done by an experienced observer who was blinded to the scanned objects. The voxel-level height threshold was $P<0.05$, and the clusterextent threshold was 20 voxels.

RNA-sequencing and transcriptomics analysis

Total RNA was extracted by Trizol (Invitrogen, USA). Ribo-Zero rRNA Removal kit (Illumina, USA) was used to remove rRNAs from the total RNA. High-quality RNA was preprocessed by TruSeq Stranded Total RNA Library Prep kit (Illumina) to construct cDNA libraries. The libraries were qualified and quantified with BioAnalyzer 2100 system (Agilent Technologies, USA). High-quality libraries were denatured into single-stranded DNA, captured on Illumina flowcell and amplified into clusters in situ, and then 150 cycle sequencing was performed on NovaSeq 6000 sequencer (Illumina). The sequencing data were imported into Gene set enrichment analysis (GSEA) software (v.4.3.3) to enrich signaling pathways. The Canonical pathways set was obtained from the MSigDB database (https://www.gsea-msigdb.org/gsea/msigdb/), and NOM P value<0.05 was considered significantly enriched [46]. The sequencing data were imported into the R platform 4.2.0, and the "DESeq2" package [47] was used to analyze the differentially expressed genes (DEGs) of the two groups. Genes with adjust P values<0.05 and |log2 (Fold change)| ≥ 1 were considered to have differential expression. DEGs were used for Gene ontology (GO) analysis, Kyoto encyclopedia of genes and genomes (KEGG) pathway analysis and protein-protein interaction (PPI) network construction. Protein-protein interaction (PPI) of DEGs was performed using STRING (https://cn.string-db.org), and PPIs with scores>0.4 were visualized as networks using Cytoscape (v3.7.1) [48]. The top 20 target proteins were scored by the maximum cliqness centrality (MCC) algorithm using plug-in CytoHubba of Cytoscape. Gene ontology (GO) analysis and Kyoto encyclopedia of genes and genomes (KEGG) pathway analysis were performed, and significantly enriched GO terms and pathways were screened according to the adjusted $P<0.05$.

Hydroxymethylated/methylated DNA immunoprecipitation (hMeDIP / MeDIP) sequencing

Genomic DNA was extracted from the hippocampus of mice in the control and IH groups using the DNeasy kit (QIAGEN, Germany) and sonicated to fragments ranging from 100 to 300 bp. Subsequently, the fragmented

DNA was end repaired with the Universal DNA Library Prep kit (GenSeq, China), adding dA tails and adaptor sequences. A portion of the DNA labeled input (about 10%) after the adaptor was added was retained, and the remaining was subjected to immunoprecipitation reaction with the 5mC MeDIP kit and 5hmC MeDIP kit (GenSeq), respectively. The Illumina PCR Primers and 2×HiFi PCR Mix (GenSeq) were used for library amplification and purification of immunoprecipitated DNA as well as Input DNA that had not been immunoprecipitated. Purified DNA libraries were quantified by Qubit (ThermoFisher) fluorescence assay and sequenced with NovaSeq 6000 sequencer.

hMeDIP-PCR

DNA samples were fragmented to 100 to 300 bp, and each sample was divided into purified immunoprecipitated DNA and input DNA. The purified DNA was used to verify the target gene. Primer sequences are shown in Supplementary Table S1.

Quantitative real-time (qRT)-PCR

Total RNA was extracted by Trizol. Reverse transcription of cDNA using PrimeScriptTM RT kit (ABM, Canada). qRT-PCR with the LightCycler 480 system (Roche, Switzerland) was performed using Maxima SYBR Green/ROX qPCR Master Mix (ABM). The relative expression level was calculated by $2-\Delta\Delta Ct$. Primer sequences are shown in Supplementary Table S1.

Cell-type annotation

According to the existing annotations of the brain in the CellMarker database (http://biocc.hrbmu.edu.cn/CellMarker/) [49], DEGs, differentially methylated/demethylated genes (DMG/DDG)-enriched cell types were marked.

DNA extraction and dot blot

The TIANamp Genomic DNA Kit (Tiangen, Beijing, China) was used to extract genomic DNA from mice hippocampus. Genomic DNA was denatured and dot onto a nitrocellulose filter membrane (Whatman, UK) and violet cross-linked. The membrane was blocked with 5% milk and then incubated with primary antibodies against 5hmC (dilution 1: 1000; Cell Signaling Technology) and 5mC (dilution 1:1000; Cell Signaling Technology) antibodies overnight at 4 °C. After washing with TBST, membrane was incubated with peroxidase-coupled secondary antibodies for 1 h at 37 °C and then developed using enhanced chemiluminescence (7sea biotech, Shanghai, China). The signals were quantified using ImageJ software. In addition, 0.02% methylene blue was stained in 0.3 M sodium acetate (pH 5.2) to visualize DNA as a total genomic DNA loading control.

Hematoxylin-eosin (HE) staining

Brain tissues were fixed in 4% paraformaldehyde for 48 h. The tissues were washed with phosphate buffered saline (PBS), dehydrated with ethanol, embedded in paraffin, and sliced. Sections were stained with H&E and examined under a light microscope (Nikon, 80i, Japan). Representative images were obtained at high magnifications of 400×.

Immunohistochemistry (IHC) staining

The tissue antigen was repaired. Sections were blocked with 5% goat serum protein and then incubated with primary antibodies against TET1 (dilution 1:500; GeneTex, USA), TET2 (dilution 1:200; Cell Signaling Technology), and TET3 (dilution 1:500; GeneTex) antibodies overnight at 4 °C. After washing with PBS, the sections were incubated with peroxidase-coupled secondary antibodies for 30 min at 37 °C. Representative images were obtained at high magnifications of 400×. Image J software was used to analyze the images.

Immunofluorescence (IF) staining

Sections were incubated with primary antibodies against TET1 (dilution 1:100; GeneTex), DCX (dilution 1:100; Cell Signaling Technology), Iba-1 (dilution 1:100; Cell Signaling Technology), GFAP (dilution 1:100; Cell Signaling Technology) antibodies overnight at 4 °C and subsequently incubated with Cy5-labeled secondary antibodies for 30 min at 37 °C. Nuclei were stained with DAPI. Representative images were observed under a fluorescence microscope (Leica, Wetzlar, Germany). Representative images were obtained at high magnifications of 400×.

Luminex liquid suspension chip analysis

Luminex liquid suspension chip analysis was performed using the Bio-Plex Pro Mouse Cytokine Grp I Panel 23-plex Assay (Bio-Rad, USA). In brief, mouse hippocampi were incubated for 30 min in 96-well plates embedded with microspheres, followed by 30 min incubation with detection antibodies. Subsequently, Streptavidin-PE was added for 10 min and values were read using the Bio-Plex 200 system (Luminex Corporation, USA).

Behavior assessment

Barnes maze

Mice were assessed for behavior 2 weeks after stereotaxic injection. Short-term and long-term spatial learning and memory were assessed using the Barnes maze [50]. The maze consisted of a circular platform with 20 holes arranged equally spaced at the edges, one of which was connected to a dark chamber, the target hole. The stimulus of light (a 200 W white light lamp) forced mice to search for the target hole. Each mouse was allowed to adapt for 2 min the day before testing. During the training

session, each mouse underwent a 4-day spatial acquisition phase in which two 3-min trials spaced 15 min apart were performed each day. Each mouse was placed in the center of the platform and covered with an opaque chamber for 5 s. The chamber was subsequently removed and the mice allowed to explore freely for 3 min. Aversive light was turned on to encourage the mouse to run and escape into the target hole. When the target hole failed to be entered within 3 min, the mice were gently guided into the target hole using a transparent chamber. Mice were allowed to explore the target hole for 1 min before being returned to their main cage and the platform cleaned with 70% ethanol. Mice were tested for short-term memory on day 5 and long-term memory on day 12. The time to find the target hole was recorded for each trial, and the trajectory was depicted using the Tracking Master system v4.0 (Beijing Zhongshi Technology Co., Ltd.).

Y-maze maze

Y-maze maze consisted of three equiangularly arranged arms, labeled A, B, and C, each 40 cm long, 5 cm wide, and 13 cm high [51]. Each mouse was placed distal to arm A and moved freely through the maze over an 8-min period, and the order and number of its arm entries were recorded. Consecutive entry into all three arms (i.e., ABC, BAC, CBA) was considered a single spontaneous alternating behavior. Percentage alternation was calculated as the ratio of actual and possible alternation (the total number of entries into the arm minus 2), multiplied by 100. The number of entering arms was used as an indicator of motor function.

Novel object recognition (NOR)

NOR was performed in an open field 0.3 m long, 0.3 m wide, and 0.45 m high [52]. Mice were trained for 5 min, during which time they were placed in the center of the arena in the presence of two identical objects. After 1 h of training, mice were replaced into the open field for testing in which one of the objects was replaced by a novel object. Time spent exploring old and new objects was quantified using the Tracking Master system v4.0. The discrimination index was calculated as $(T_{novel} - T_{Familiar}) / (T_{Novel} + T_{Familiar})$.

In addition, Pearson correlation analysis was performed between behavioral data and global 5hmC levels, Wnt pathway gene expression levels and their 5hmC levels in the hippocampus, and $P<0.05$ represented a significant correlation.

Statistical analysis

All data are in average±standard deviation (SD) and repeated at least 3 times. Pearson correlation analysis was performed using SPSS software (v.25). Other data were analyzed using GraphPad Prism v. 9.4. The differences between the groups were determined by the student T-test (two groups) or one-way analysis of variance (ANOVA). *P* values<0.05 for difference was statistically significant.

Results

IH exposure induced the upregulation of TETs and total 5hmC in the hippocampus of mice

The IH mouse model was established as described in previous studies (Fig. 1A). At the end of the 4th week of IH, weight, PO_2 and fMRI were measured in the control and IH groups. The body weight and hippocampal PO_2 in the IH group were significantly lower than those in the control group (Fig. 1B). fMRI analysis of the IH mice revealed significantly lower BOLD signal activation in the hippocampus, especially on the left side, than in the control mice (Fig. 1C). Previous studies have shown that TETs mediated 5hmC modification plays an important role in regulating cognitive function. At the end of the 6th week of IH, the hippocampal tissues of the control and IH groups were collected for DNA dot blot, IHC staining and qPCR. The total amount of 5hmC in the hippocampus of control and IH mice was quantified using DNA dot blot analysis. As shown in Figs. 1D and 5hmC levels were significantly increased by IH compared with those in the controls. We determined the expression of TET1, TET2 and TET3 enzymes in the hippocampus by IHC and qPCR. As shown in Fig. 1E, compared with those in the controls, the mRNA expression levels of *Tet1*, *Tet2*, and *Tet3* in the IH group increased significantly. Interestingly, *Tet1* level increased approximately 2-fold. Meanwhile, the protein expression levels of TET1, TET2 and TET3 were also increased in the hippocampal dentate gyrus of IH mice (Fig. 1E). Overall, IH induced the expression of DNA hydroxymethyltransferase TET and modification of global 5hmC.

IH exposure caused DEGs in the hippocampus of mice

At the end of the 6th week of IH, the hippocampal tissues of the control and IH groups were collected for RNA-seq and hMeDIP/ MeDIP-seq. The hMeDIP-seq process is shown in Fig. 2A. To evaluate the effect of IH on the hippocampus, the hippocampi of the control and IH mice were subjected to transcriptome sequencing. A total of 253 signaling pathways were enriched by GSEA (NOM *P* value<0.05), including those related to cell cycle (e.g. cellcycle pathway and cyclin A B1 B2 associated events during G2 transition) and neuroregulation (e.g. TYROBP causal network in microglia and dopaminergic neurogenesis) (Supplementary Figure S1, Supplementary Table S2). In addition, MAPK pathway and hypoxia via HIF1A dn were also enriched. A total of 3263 DEGs were identified, including 1 309 upregulated DEGs and 1 954 downregulated DEGs (Supplementary Table S3).

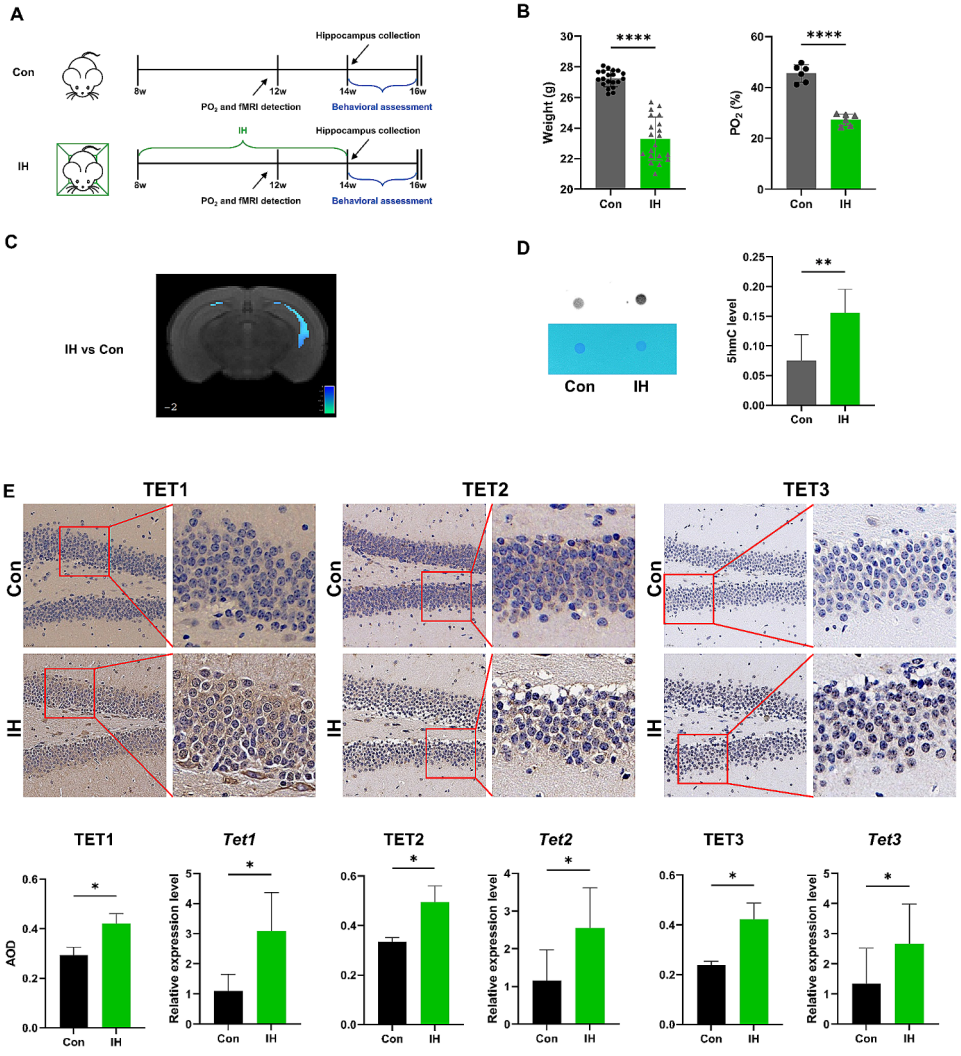

Fig. 1 IH exposure induced the upregulation of TETs and total 5hmC in the hippocampus of mice. (**A**) The illustration of IH modeling. (**B**) Body weight and hippocampal PO_2. (**C**) BOLD-fMRI analysis of the hippocampus. (**D**) Total amount of 5hmC in the hippocampus using standard DNA dot blot. (**E**) The expression of TET1, TET2, and TET3 in the hippocampus using IHC staining and qPCR. Analysis was performed by Student's t test. All data are presented as the mean ± standard deviation

Hierarchical clustering and volcano plot were used to analyse the DEGs and visualize the genomic data (Fig. 2B, Supplementary Figure S2A). STING and Cytoscape were used to construct the PPI network and visualization, and the CytoHubba plugin with MCC algorithm was used to score and rank the target proteins. The top 20 target proteins are mostly related to cell cycle (e.g., Cdk1, Ccnb1, Bub1) or Wnt (e.g., Wnt3a, Wnt2) (Supplementary Figure S2B). GO and KEGG pathway enrichment analyses were subsequently performed using the DEGs. A total of 1 703 GO terms were obtained, including 3 676 BP, 303 CC, and 573 MF (adjusted *P* value < 0.05) (Supplementary Table S4). As shown in Fig. 2C, compared with those in the controls, the regulated transcripts in the hippocampi of IH mice were associated with the BP terms axonogenesis, axon guidance, and the pattern specification process, MF terms, such as ion and gated channel activity, and in CC terms, such as the synaptic membrane and ion channel complex. A total of 67 Signaling pathways were enriched according to KEGG pathway analysis (adjusted *P* value < 0.05) (Supplementary Table S5). Twenty pathways, including neuroactive ligand–receptor interaction, the cAMP Signaling pathway, the Wnt Signaling pathway, and the MAPK Signaling pathway, were screened for visualization based on the P value (Fig. 2D). These results showed that IH altered the expression of inflammatory- and neuroactive-related genes in the hippocampus.

IH exposure caused DMG/DDG in the hippocampus of mice

MeDIP-seq and hMeDIP-seq were performed on 5mC and 5hmC, respectively, to map the genome differences between the hippocampi of control and IH mice. As

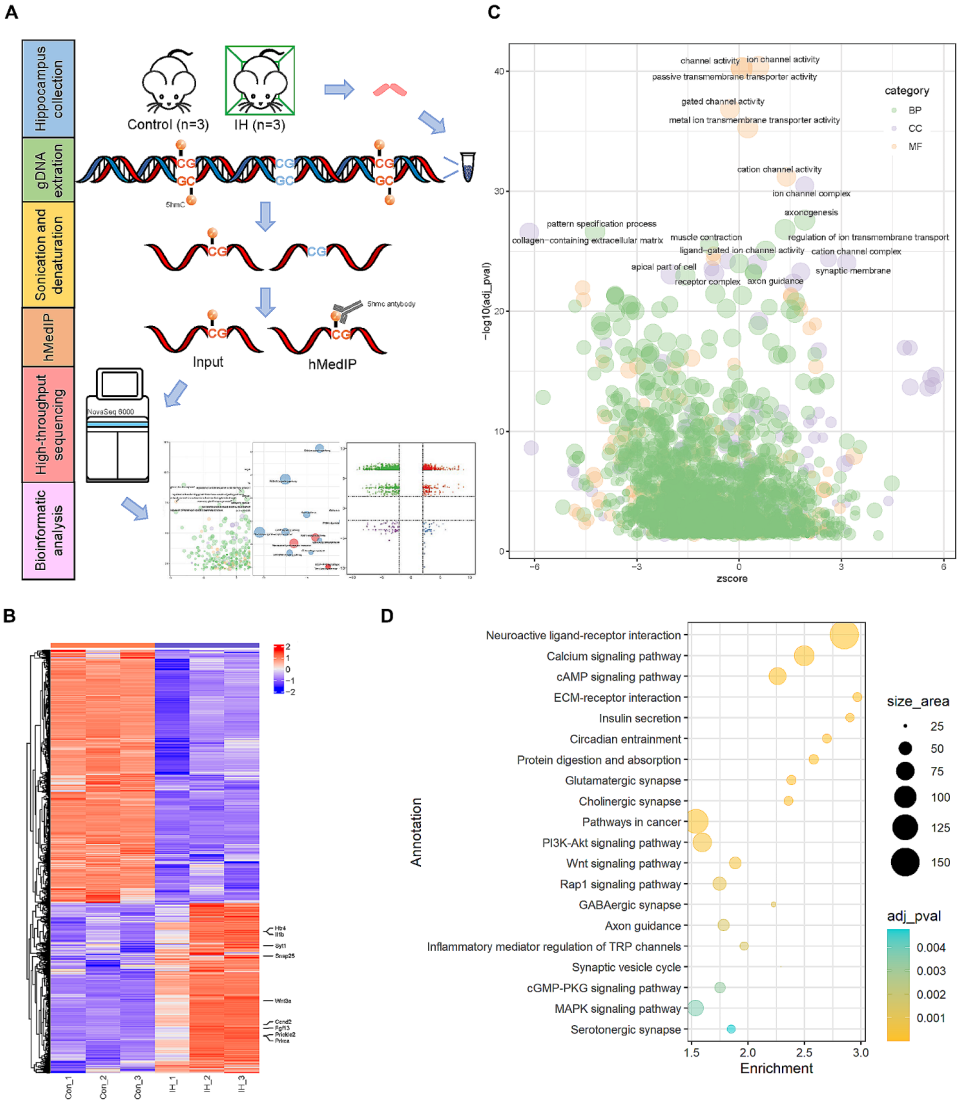

Fig. 2 IH exposure caused DEGs in the hippocampus of mice. (**A**) The illustration of hMeDIP-sequencing. (**B**) DEGs were displayed by hierarchical clustering. (**C**) GO enrichment. (**D**) KEGG pathway enrichment

shown in Fig. 3A, there were significant differences in the mean normalized counts of 5mC- and 5hmC-enriched regions in the hippocampus between control and IH mice. Heatmap clustering was used to visualize the 5 kb distribution of 5mC and 5hmC peaks upstream and downstream of the transcription start site (TSS) (Fig. 3B). Compared with control mice, IH mice presented decreased enrichment of 5mC in this genomic region, whereas the corresponding level of 5hmC increased (Fig. 3C). Genes containing altered 5hmC peaks were analysed, and 12 606 genes were found to be differentially demethylated in the hippocampus between control and IH mice; 10 994 of these genes were demethylated, and 1 612 were not demethylated (Supplementary Table S6). GO analysis of the DDGs revealed a total of 5 824 enriched GO items, including 4 723 BP, 392 CC, and 709 MF terms (Supplementary Table S7). According to the adjusted *P* value, 30 GO terms were screened for visual analysis (Fig. 3D). The results of the BP analysis indicated that DDGs were mainly enriched in terms related to axonogenesis, synapse organization, and cell junction assembly terms. In the MF, the most enriched terms included GTPase regulator activity, nucleotide-triphosphatase regulator activity, and metal ion transmembrane transporter activity. The three most enriched CC terms were glutamatergic synapse, neuron to neuron, and synapse asymmetric synapse. Genes containing altered 5mC peaks were analysed, and 16 033 genes were found to be differentially methylated in the hippocampus between control and IH mice, 15 620 of which were methylated and 413 of which were unmethylated (Supplementary Table S8). GO analysis of the DMGs revealed a total of 4 732

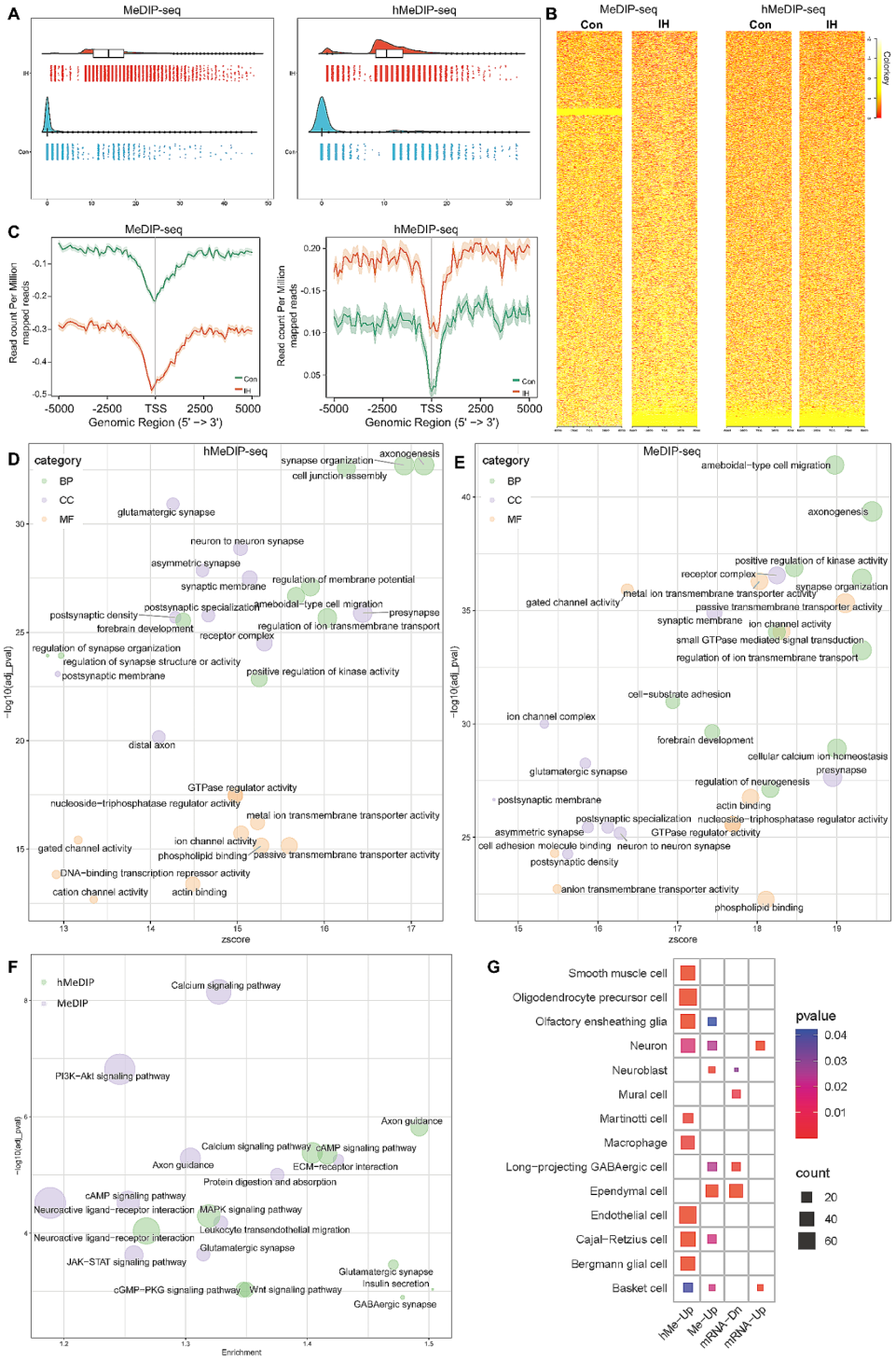

Fig. 3 IH exposure caused DMG / DDG in the hippocampus of mice. (**A**) Mean normalized counts of 5mC- and 5hmC-enriched regions in the hippocampus. (**B**) (**C**) 5 kb distribution of 5mC and 5hmC peaks upstream and downstream of the TSS. (**D**) GO analysis of the DDGs. (**E**) GO analysis of the DMGs. (**F**) KEGG pathway analysis. (**G**) Cell types enrichment

enriched GO items, including 3 977 BP, 288 CC, and 467 MF terms (Supplementary Table S9). According to the adjusted *P* value, 30 GO terms were screened for visual analysis (Fig. 3E). The BP results indicated that DMGs were mainly enriched in ameboidal-type cell migration, cell junction assembly and axonogenesis terms. In the MF, the most enriched terms included metal ion transmembrane transporter activity, gated channel activity,

and passive transmembrane transporter activity. The three most enriched CC terms were collagen-containing extracellular matrix, receptor complex, and synaptic membrane. Moreover, they were enriched in CCs such as receptor complexes and synaptic membranes. KEGG analysis of the DDGs and DMGs revealed 121 and 123 enriched Signaling pathways, respectively (Supplementary Table S10, Supplementary Table S11). According to the adjusted P value, 10 pathways were screened separately for visualization; among these pathways, the DDG-enriched pathways included axon guidance, the cAMP Signaling pathway, and the Wnt Signaling pathway, and the corresponding DMGs included the calcium Signaling pathway, the PI3K-Akt Signaling pathway, and axon guidance (Fig. 3F). The cell types enriched in the upregulated and downregulated DEGs, upregulated DDGs, and upregulated DMGs are marked. As shown in Fig. 3G, the upregulated DEGs were enriched mainly in neurons and basket cells, and the downregulated DEGs were enriched mainly in ependymal cells and the other 4 cell types. The upregulated DMGs were enriched mainly in ependymal cells and the other 7 cell types, and the upregulated DDGs were enriched mainly in 10 cell types, including smooth muscle cells, Cajal–Retzius cells, olfactory ensheathing glia, oligodendrocytes, endothelial cells and Bergmann glial cells. These data indicated that IH induced global enrichment of 5hmC markers, especially in genes related to inflammation and neural activity.

IH exposure promoted the binding of 5hmC to wnt pathway genes in the hippocampi of mice

Given the critical function of 5hmC alterations in controlling gene expression, we investigated the relationship between 5hmC and mRNA levels. Supplementary Figure S3A shows the proportion of 5mC and 5hmC peaks in each genomic region. Significant differences were found by comparing the enrichment of 5mC and 5hmC in promoter regions in the hippocampus of control and IH mice (Supplementary Figure S3B). The RNA-sequencing data was combined with the methylation, demethylation and gene expression in promoter regions data (Fig. 4A, Supplementary Table S12, S13). Compared with those in the control group, the expression and demethylation levels of genes involved in the Wnt (*Wnt3a*, *Ccnd2* and *Prickle2*), synaptic vesicle cycle (*Snap25*, *Syt1*), MAPK (*Il1b*, *Fgf13*) and cAMP (*Htr4*, *Adcy1*) Signaling pathways were increased. The expression of the above genes in the hippocampi of control and IH mice was examined by qPCR. The results showed that the above genes were upregulated after IH stimulation (Fig. 4B). 5hmC profiles revealed high 5hmC levels during IH treatment (Fig. 4C, Supplementary Figure S4). The demethylation levels of specific regions in *Wnt3a*, *Ccnd2* and *Prickle2* were validated by hMeDIP-qPCR. The results showed that IH stimulation increased the binding of the above genes to 5hmC (Fig. 4D). These findings suggested that 5hmC modification may play an epigenetic regulatory role in the expression of *Wnt3a*, *Ccnd2* and *Prickle2* in the Wnt pathway in the hippocampi of IH-treated mice.

Tet1 intervention improved hippocampal cognitive dysfunction in IH mice

Taken together, our data demonstrate that the expression of DNA hydroxymethyltransferases, especially TET1, is significantly altered in the hippocampus of IH mice, suggesting a critical role for DNA hydroxymethylation. To investigate IH further, we altered the DNA hydroxymethylation levels in the hippocampus by knocking down *Tet1* using a lentivirus plasmid (Fig. 5A). IH mice treated with shNC or sh*Tet1* are shown in Fig. 5A. Figure 5B illustrates the design of the lentivirus carrying sh*Tet1*. 293T cells were transfected with shNC or sh*Tet1* for 72 h, and green fluorescence was observed under a high-content microscope, confirming successful transfection (Supplementary Figure S5). The qPCR results showed that the *Tet1* mRNA level in N2A cells transfected with sh*Tet1* was significantly lower than that in N2A cells transfected with shNC, while there was no significant difference between the shNC-transfected cells and the control cells (Fig. 5C). At the end of the 6th week of IH, hippocampal tissues were collected for IHC staining, qPCR and IF staining. IHC and qPCR showed that both the staining and relative mRNA expression of total TET1 in the hippocampus of sh*Tet1*-treated mice were significantly lower than those in the IH group (Fig. 5D). IF staining demonstrated the subcellular localization of TET1 in the hippocampus, and the localization changes after IH treatment and *Tet1* knockdown (Fig. 5E). Hippocampus is an important brain region responsible for encoding and storing memories. Thus, behavioral assessments, including Barnes maze, Y maze, and NOR tests, were performed during weeks 6 to 8 of IH. The exploratory trajectories of the Barnes maze-treated mice on Days 5 and 12 showed that the short-term and long-term memory deficits, respectively, were impaired after IH exposure but recovered after *Tet1* knockdown (Fig. 6A). The latency to identify target box was significantly greater in the IH group than in the control group, while it was significantly lower in the IH+sh*Tet1* group than in the IH group (Fig. 6B). Figure 6C shows the changes in latency to reach the target box during the 4-day training period in each group of mice. The Y-maze test showed that spontaneous alternation behaviour was significantly lower in the IH group than in the control group but was significantly greater in the IH+sh*Tet1* group than in the IH group (Fig. 6D). There was no significant difference in the total number of arm entries between the groups, suggesting that the changes in spontaneous alternation behaviour were not

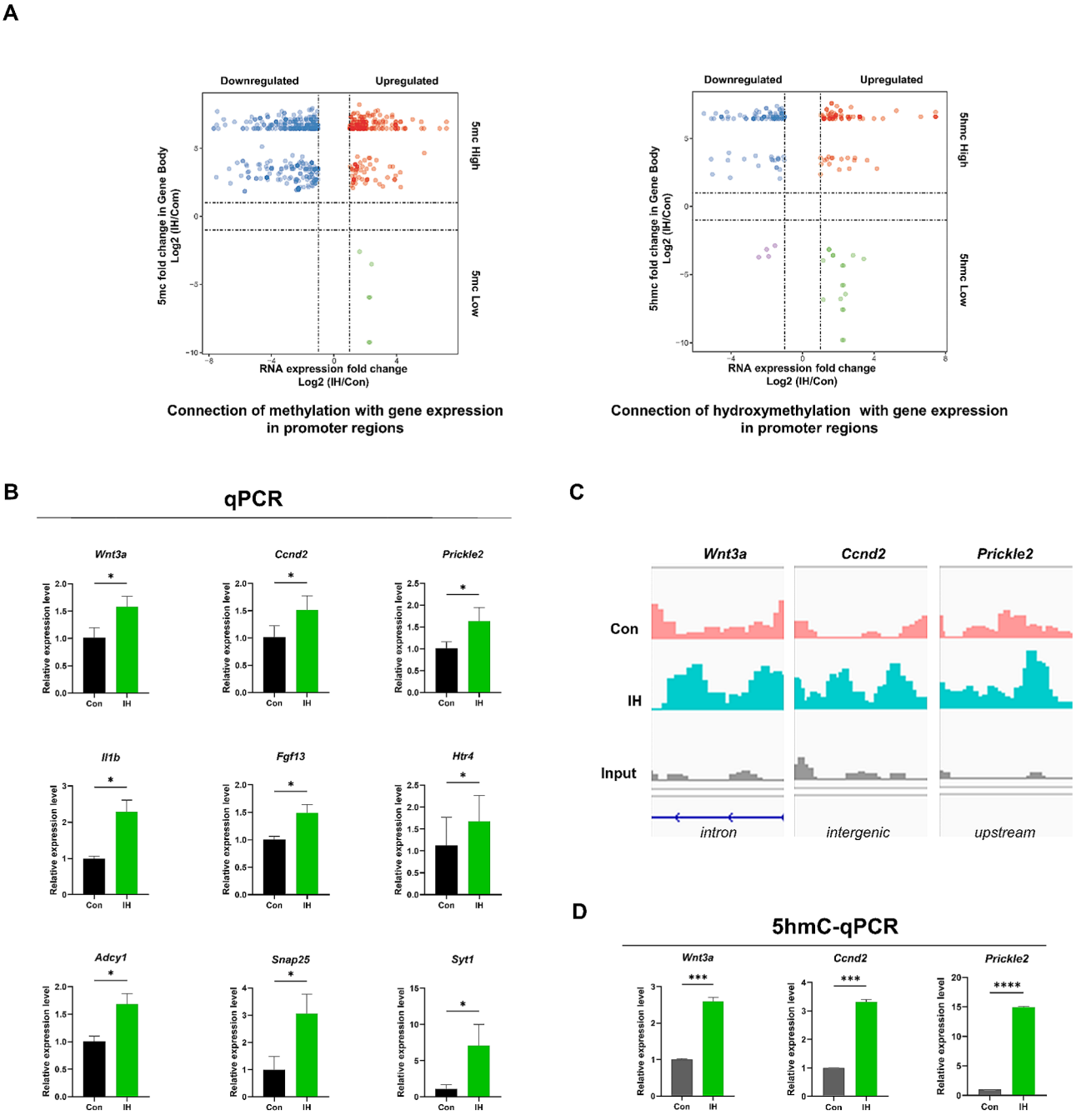

Fig. 4 IH exposure promoted the binding of 5hmC to Wnt pathway genes in the hippocampi of mice. (**A**) The connection by assimilating RNA-sequencing data into methylation, demethylation and gene expression in promoter regions. (**B**) The expression of *Wnt3a*, *Ccnd2*, *Prickle2*, *Il1b*, *Fgf13*, *Htr4*, *Adcy1*, *Snap25*, and *Syt1* in the hippocampus using qPCR. (**C**) 5hmC profiles of *Wnt3a*, *Ccnd2*, and *Prickle2*. (**D**) The demethylation levels of specific regions in *Wnt3a*, *Ccnd2* and *Prickle2* using hMeDIP-qPCR. Analysis was performed by Student's t test. All data are presented as the mean ± standard deviation

due to motor deficits (Fig. 6E). The NOR test showed that the preference of mice for new objects was significantly lower in the IH group than in the control group but was significantly greater in the IH + sh*Tet1* group than in the IH group (Fig. 6F). There was no significant difference in the total interaction time with old or new objects between the groups, suggesting that the changes in the discrimination index were not due to lack of interest (Fig. 6G). These findings suggested that *Tet1* knockdown can ameliorate the short-term and long-term memory impairment caused by IH. Besides, Pearson correlation analysis was performed between cognitive function and global 5hmC levels, Wnt pathway gene expression levels and their 5hmC levels. As shown in Table 1, latency to

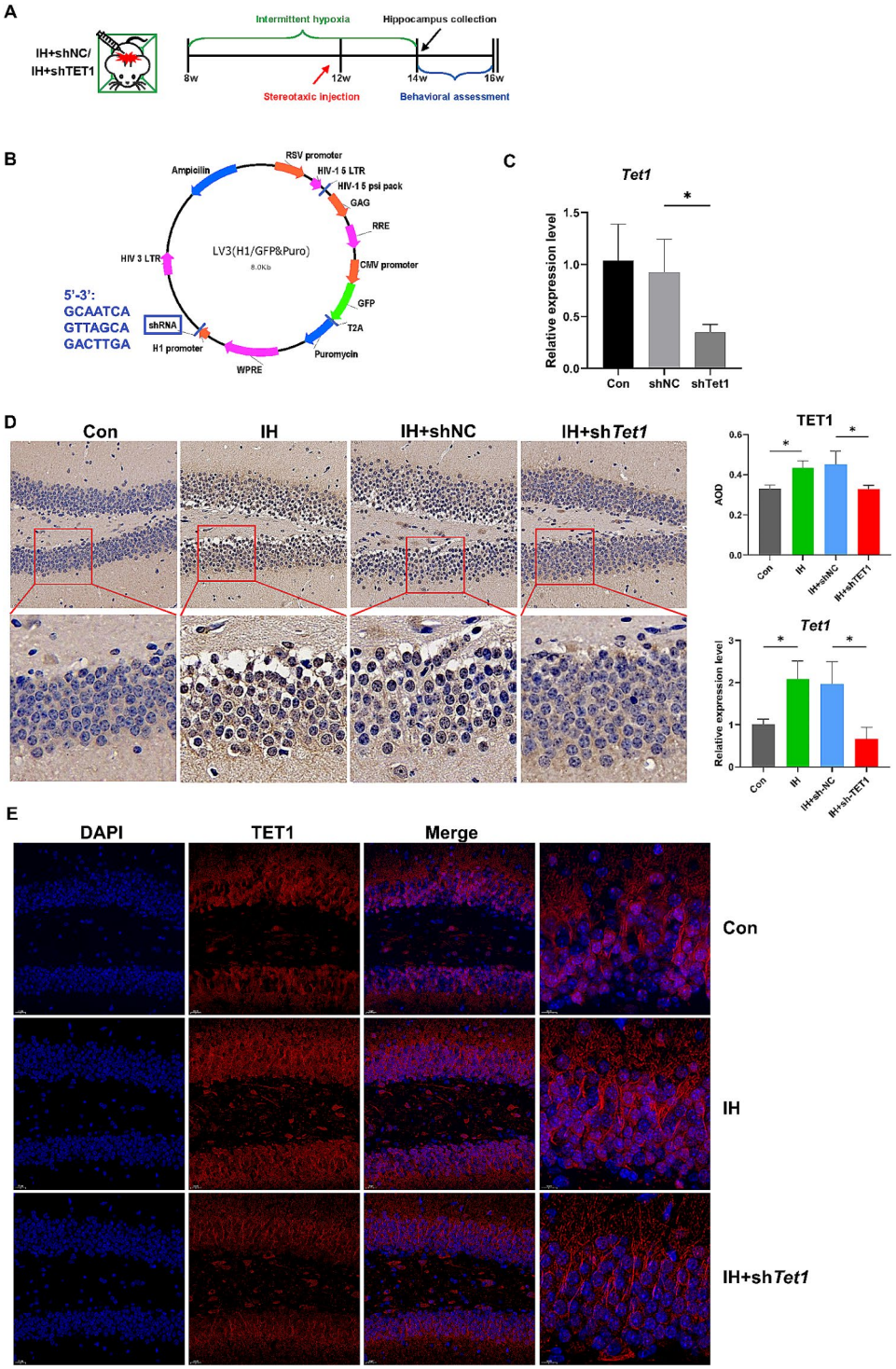

Fig. 5 *Tet1* knockdown was effective in vitro and in vivo. (**A**) The illustration of *Tet1* intervention. (**B**) The design of the lentivirus carrying sh*Tet1*. (**C**) The expression of *Tet1* in N2A cells using qPCR. (**D**) The expression of TET1 in the hippocampus using IHC staining and qPCR. (**E**) The subcellular localization of TET1 in the hippocampus using IF staining. Analysis was performed by Student's t test. All data are presented as the mean ± standard deviation

identify target box at day 5 in the Barnes maze was significantly positively correlated with global 5hmC levels and *Prickle2* mRNA expression. The proportion of alternating behaviors in the Y-maze was negatively correlated with the mRNA levels of *Wnt3a*, *Ccnd2*, and *Prickle2*, as well as the 5hmC levels of *Wnt3a* and *Prickle2*. The discrimination index in the NOR was significantly positively correlated with the 5hmC level of *Wnt3a*.

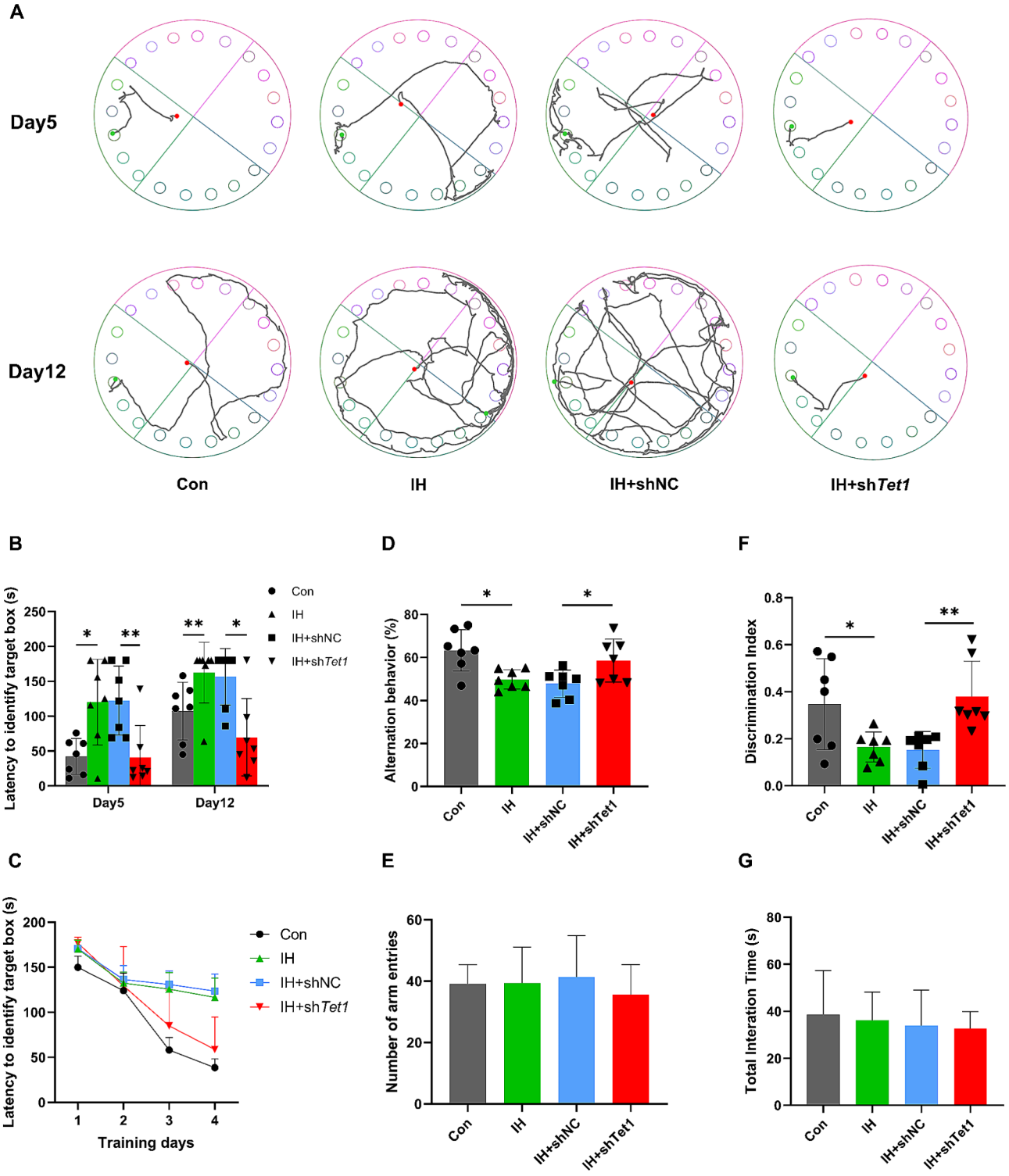

Fig. 6 *Tet1* intervention improved hippocampal cognitive dysfunction in IH mice. Measured in the Barnes maze: (**A**) Exploratory trajectories on days 5 and 12. (**B**) Latency to identify target box on days 5 and 12. (**C**) Latency to identify target box during the 4-day training period. Measured in the Y-maze: (**D**) Alternation behavior. (**E**) Number of arm entries. Measured in the NOR: (**F**) Discrimination index. (**G**) Total interaction time. Analysis was performed by Student's t test. All data are presented as the mean ± standard deviation

Table 1 Correlation analysis of the cognition function and 5hmC demethylation

	Latency to identify target box on the 5th day of the Barns maze	Latency to identify target box on the 12th day of the Barns maze	Alternation behaviors of the Y-maze	Discrimination index of the NOR
global 5hmC level	0.816*	0.219	-0.52	-0.397
5hmC level of Wnt3a	0.766	0.7	-0.850*	-0.754
mRNA level of Wnt3a	0.782	0.773	-0.919**	-0.824*
5hmC level of Ccnd3	0.799	0.695	-0.852*	-0.762
mRNA level of Ccnd2	0.37	0.747	-0.77	-0.735
5hmC level of Prickle2	0.809	0.715	-0.854*	-0.762
mRNA level of Prickle2	0.898*	0.28	-0.838*	-0.736

*$p<0.05$ ** $p<0.01$

Tet1 knockdown limited excessive wnt signaling activation and hippocampal neurogenesis in mice

Wnt pathway plays a crucial role in regulating neurogenesis and neuroinflammation, and its dysregulation can lead to various neuropathologies. While moderate neurogenesis and neuroinflammation have positive effects on the brain; however, their excess is often catastrophic. In this study, brains were collected at the end of the 6th week of IH for HE staining of hippocampal CA1, CA3 and DG regions. As illustrated in Fig. 7A, the neurons in the hippocampi of control mice were well-organized, clearly stained, and exhibited a normal microstructure under normal oxygen conditions. In contrast, the IH group showed evident pathological changes; the neurons appeared loosely arranged with light staining, and there was observed neuron loss and nuclear pyknosis. However, following treatment with sh*Tet1*, the morphology of all tissues tended to normalize. Then, we utilized DNA dot blot and qPCR to assess the global 5hmC levels and Wnt pathway gene expression. Our findings revealed a decrease in the 5hmC level in the hippocampi of sh*Tet1* mice compared to IH mice, as determined by standard dot blot (Fig. 7B). The mRNA levels of *Wnt3a*, *Ccnd2*, and *Prickle2* were significantly lower in the hippocampi of sh*Tet1* mice compared to IH mice, as determined by qPCR (Fig. 7C). Additionally, sh*Tet1* injection significantly reduced IH-induced demethylation levels of specific regions in *Wnt3a*, *Ccnd2*, and *Prickle2*, as determined by hMeDIP-qPCR (Fig. 7D). Finally, IF staining was used to examine the expression of DCX (a marker of immature neurons) in the hippocampal DG area (Fig. 7E). Quantitative analysis revealed that IH treatment significantly increased DCX expression, while it was significantly reduced after sh*Tet1* injection. These results indicated that *Tet1*-targeted therapy may effectively counteract IH-induced abnormal hippocampal neurogenesis by potentially regulating excessive levels of 5hmC and Wnt pathway genes.

Tet1 knockdown alleviated IH-induced hippocampal neuroinflammation in mice

We then investigated n hippocampal neuroinflammatory changes in the hippocampus following IH, as well as improvements observed after sh*Tet1* injection. IF staining was utilized to assess the expression of IBA1 (a marker of microglia) and GFAP (a marker of astrocytes) in the hippocampal DG area (Fig. 8A-B). Quantitative analysis revealed that IH treatment significantly elevated the expression of IBA1, and GFAP. Following shTet1 injection, there was a significant decrease in GFAP expression, while IBA1 showed a tendency towards reduction, although not statistically significant. Luminex liquid suspension chip analysis was used to compare the differential expression of 23 cytokines in the hippocampus of the control group, IH group and IH+sh*Tet1* group (Fig. 8C). Thirteen cytokines were significantly upregulated after IH, and the five most upregulated proteins were MIP1a, IL17A, KC, IL3 and IL12 (p40). The expression of eight cytokines, such as TNFa, IL3, IL9 and IL17A, decreased significantly after sh*Tet1* injection (Fig. 8C, Supplementary Table S14). Taken together, these data indicate that *Tet1*-targeted therapy may be effective against IH-induced hippocampal inflammation, possibly also by limiting the excessive levels of 5hmC and Wnt pathway genes.

Discussion

IH is an important feature of OSA and plays a major role in hippocampal oxidative stress injury and cognitive dysfunction [53]; however, the exact mechanism involved remains poorly understood. In this study, for the first time, we revealed the effects of IH on the DNA demethylation process in the mouse hippocampus and linked these effects with changes in hippocampus-related cognitive functions. In addition, we found that IH regulated neuroinflammation and neurogenesis through the demethylation of Wnt Signaling pathway genes, which was reversed by *Tet1* knockdown.

The enzymatic activity of TETs, members of the 2-OGDD superfamily, may be regulated by oxygen

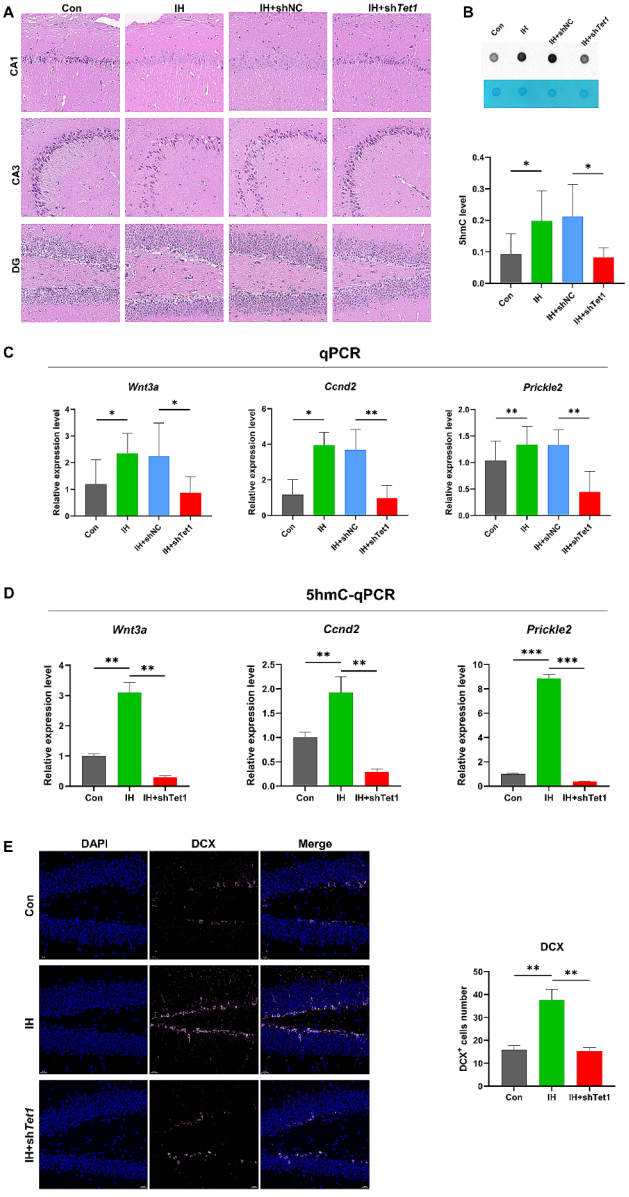

Fig. 7 *Tet1* knockdown increased hippocampal microglia. (**A**) Hippocampal morphology using HE staining. (**B**)(**C**)(**D**) The expression of DCX, GFAP and IBA1 in the hippocampus using IF staining. Analysis was performed by Student's t test. All data are presented as the mean ± standard deviation

availability and redox-based mechanisms, thereby catalysing the progressive oxidation of 5mC from DNA [54, 55]. Unlike those of Tet2 and Tet3, the enzymatic activity of Tet1 is more sensitive to changes in oxygen concentration within the physiological hypoxic range. Specifically, Oxygen-dependent Tet1 activity mediates the phasic burst of 5hmC levels during early differentiation in vitro [56]. In various tumor cell lines, hypoxia leads to reduced 5hmC levels by decreasing the activity of TET enzymes without concomitant TET expression [28]. It should be noted that the inhibition of the DNA hydroxymethylation process was observed only at oxygen concentrations below about 2%. The IH used in our study is a specific chronic mild hypoxia with alternating oxygen concentrations from 5 to 21%, most likely far from sufficient to inhibit TET enzyme activity. On the other hand, hypoxia induces transcriptional activation of *TET1* but not *TET2* or *TET3* in a variety of neuroblastoma cell lines, resulting in elevated global 5hmC levels and enrichment of 5hmC at canonical hypoxia response genes. This reflected the oxygen-dependent non-enzymatic function of *TET1* [28, 30]. 5hmC is a stable epigenetic marker that generally promotes gene expression [57, 58]. 5hmC is most abundant in the central nervous system, and its continuous increase in the hippocampus and other brain regions of mice from early postnatal to adulthood and possibly into old age indicates its close association with brain function and disease [58, 59]. In our study, TETs expression and total 5hmC levels were significantly higher in the hippocampi of IH mice than in those of control mice. These results suggested that TETs play, at least in part, a direct nonenzymatic role under IH, that is, by upregulating their expression to raise 5hmC levels.

Among TET enzymes, TET1 has been the earliest and most studied in the field of neuroscience, and its influence on neurogenesis extends throughout prenatal, juvenile and adult life. First, both catalytic and non-catalytic functions of TET1 drive the differentiation of mouse embryonic stem cells into neural precursors [60]. Then, TET1 can accelerate neurogenesis during mouse embryonic brain development [61]. Besides, 5hmC specifically accumulates in the Tet1-binding region during abnormal cortical development in mice at young ages, which may further affect neurodevelopment and brain function [62]. Tet1 can even control adult hippocampal neurogenesis in mice, further regulating psychological behavior and cognitive function [26, 63]. However, the effect of TET1 on cognitive function is quite controversial, and both its loss and overexpression have been reported to enhance or impair memory by mediating DNA hydroxymethylation, which may be partially attributed to the differential regulation of its two isoforms in neurons and neuroglia cytes, respectively [18, 23–27]. $Tet1^{S}$ is highly enriched in neurons, and its repression enhances hippocampus-dependent memory in mice, whereas $Tet1^{FL}$ is more abundant in glial cells, and its repression impairs memory [27]. However, overexpression of *Tet1* specifically in hippocampal CA1 pyramidal cells caused memory impairment [25]. In addition, *Tet2* also has cell type specificity in regulating cognitive processes, as its loss in adult neural progenitor cells impairs neurogenesis and cognitive function, whereas its loss in neurons enhances hippocampus-dependent memory by modulating synaptic plasticity [64, 65]. Loss of *Tet3* in brain neurons impairs hippocampal spatial orientation and short-term memory [19, 66]. Therefore, we hypothesized that IH-induced

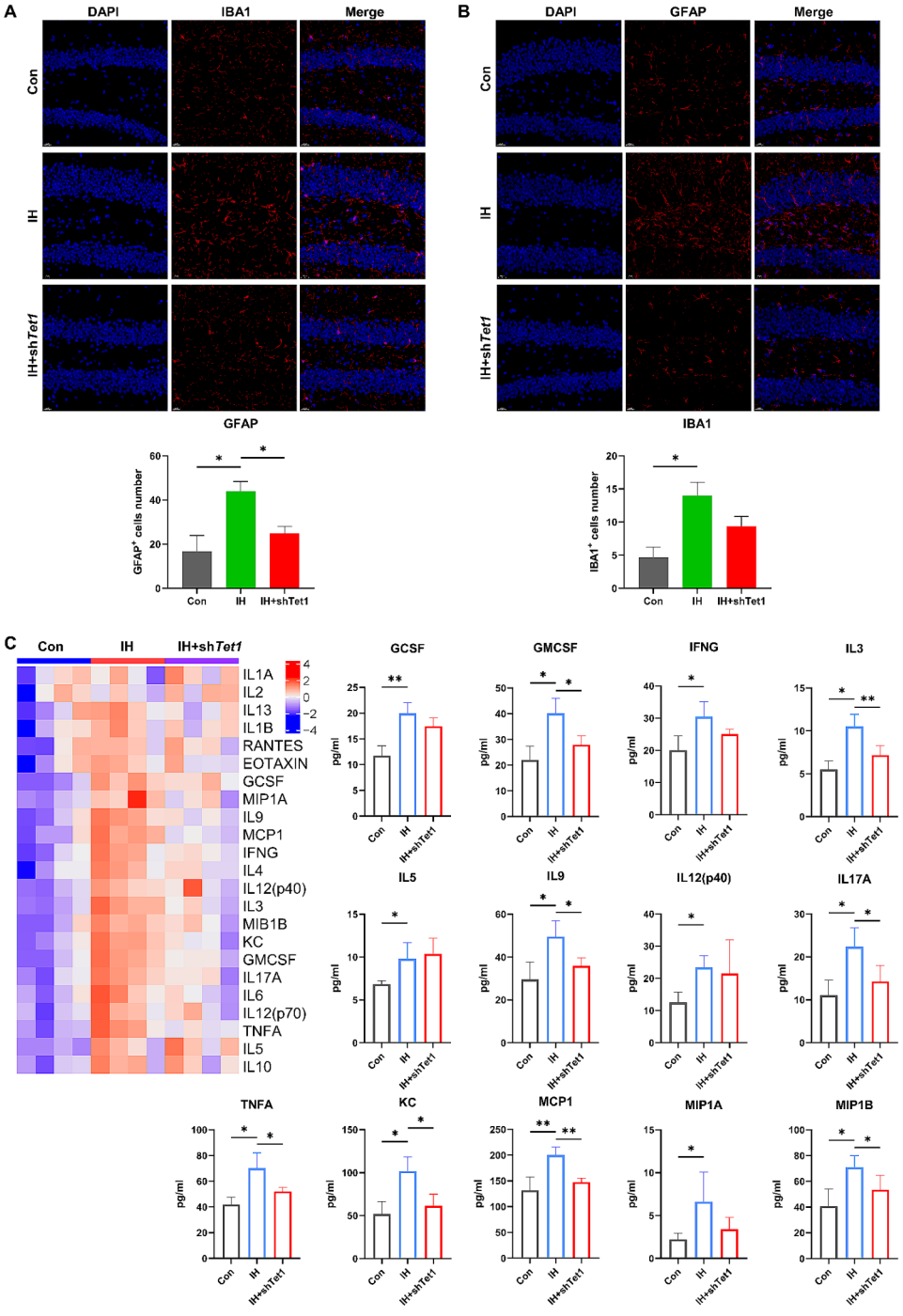

Fig. 8 *Tet1* knockdown alleviated IH-induced hippocampal neuroinflammation in mice. (**A**) The expression of *Wnt3a*, *Ccnd2*, and *Prickle2* in the hippocampus using qPCR. Analysis was performed by Student's t test. All experiments were repeated at least three times. All data are presented as the mean ± standard deviation. (**B**) Total amount of 5hmC in the hippocampus using standard DNA dot blot. (**C**) Differential expression of 23 cytokines was displayed by hierarchical clustering, and 13 of them were significantly upregulated after IH. Analysis was performed by Student's t test. All data are presented as the mean ± standard deviation

cognitive dysfunction may be associated with enhanced global DNA hydroxymethylation in the hippocampus. We found that IH mice exhibited significant decreases in spatial learning and short-term and long-term memory. Pathological changes were found in the hippocampus by HE staining, and a decreased BOLD signal was found by fMRI, especially on the left side of the hippocampus. We will further investigate the reasons for this bilateral asymmetry in the future. Furthermore, we conducted cell type annotation of DDGs and found that IH-induced 5hmC

was extensively enriched in neurons, a variety of glial cells, smooth muscle cells, and endothelial cells. Interestingly, IF staining revealed that TET1 was not expressed throughout the DG. Even if its expression was significantly upregulated after IH, it remained relatively weak in specific cells. This finding contradicts previous literature which reported high levels of TET1 expression in neurons throughout the hippocampus. In the future, it will be necessary to investigate colocalization of TET1 with different cell types in the hippocampus in the future.

Studies have shown that IH can cause hippocampal inflammatory damage and subsequent cognitive dysfunction, which may be mediated mainly by microglia [11, 67, 68]. We found several signaling pathways that were enriched in the DDGs and DEGs. These genes were found to be involved in neuroregulation -related pathways, including axon guidance, neuroactive ligand−receptor interaction, and Calcium signaling pathways, as well as inflammation -related pathways, such as MAPK signaling pathways, NF-κB signaling pathways and Th17 cell differentiation. Strikingly, the Wnt signaling pathway, which is considered to regulate neurogenesis, neuroinflammation [37], was also enriched. In addition, the top 20 key target proteins obtained by PPI analysis were mostly related to cell cycle and Wnt. The Wnt signaling pathway is divided into the canonical Wnt/β-catenin pathway and the noncanonical Wnt signaling pathway, which include the Ca^{+} pathway and PCP pathway [69]. Neurogenesis, a highly dynamic process that continues throughout the lifetime in rodents and humans, plays an important role in hippocampus-dependent learning and memory [70]. Loss of normal neurogenesis or the generation of abnormal neurogenesis can disrupt hippocampal neural circuits, leading to cognitive dysfunction [71]. The Wnt signaling pathway is the main factor controlling adult hippocampal neurogenesis, and proper Wnt signaling pathway activation is required to regulate the proliferation, differentiation and maturation of neurons [36, 72]. During the early stages of neurogenesis, canonical Wnt Signaling determines cell proliferation and maturation and subsequently, together with noncanonical Wnt signaling, regulates differentiation and morphological development [73–75]. In the canonical Wnt pathway, Wnt3a, an upstream gene, promotes neurogenesis by shortening the cell cycle of hippocampal neural progenitor cells [76]. Its downstream gene, Ccnd2, whose knockdown caused a defect in progenitor cell proliferation almost completely abolished adult neurogenesis [77]. Prickle2, a member of the non-canonical Wnt pathway, was found to be deficient in dendritic branching, synapse number and postsynaptic density [78]. However, excessive activation of this pathway may impair the maturation of neurons, causing dendrite, spine and synapse dysplasia [75, 79, 80]. The effect of the Wnt signaling pathway on neuroinflammation is mainly achieved by regulating microglial activation. In a variety of CNS diseases, microglial activation mediated by canonical Wnt signaling is generally characterized by an anti-inflammatory protective effect, while noncanonical Wnt signaling -mediated microglial activation is proinflammatory and promotes disease progression [81–88].

Even if, for instance, Wnt/β-catenin activity coincides with early neuronal damage and microglial inflammation in the hippocampi of mice with experimental autoimmune encephalomyelitis, this change can be interpreted as active inflammation activating Wnt signaling, triggering hippocampal neurogenesis, and replenishing damaged neurons [89]. However, *Wnt3a* plays dual regulatory roles in microglial and may be related to the activation of other inflammatory pathways. Intraventrically injected GSK3β inhibitors to activate canonical signaling pathways in premature rabbits with intraventricular haemorrhage inhibited microglial inflammation, while *rt-Wnt3a* promoted inflammation [90]. In vitro, *Wnt3a* can convert microglia to a proinflammatory phenotype, probably through its activation of the ERK1/2 pathway in addition to the canonical Wnt pathway [91, 92]. Activation of the NF-κB pathway can be observed when a Wnt/β-catenin pathway agonist is added to microglia, and vice versa; this bidirectional positive feedback effect may cause sustained activation of both pathways and exacerbate inflammatory damage [93]. In addition, activated microglia can also enhance the neurotoxicity of astrocytes by secreting a variety of inflammatory mediators to jointly drive inflammatory damage in the CNS [11, 94]. Therefore, we identified *Wnt3a*, *Prickle2* and *Ccnd2* in the Wnt signaling pathway as key demethylation regulators and demonstrated increased demethylation and gene expression in the hippocampi of IH mice. The level of DCX (a marker of immature neurons) in the DG region of the hippocampus were significantly increased after IH, indicating abnormal hippocampal neurogenesis. Besides, the levels of IBA1 (a marker of microglia) and GFAP (a marker of astrocytes) in the DG region of the hippocampus were significantly increased after IH. Additionally, a variety of inflammatory cytokines were significantly upregulated, indicating a neuroinflammatory state in the hippocampus.

To summarize, we heve decided to validate the induced phenotypic changes by eliminating demethylation via hippocampus-specific knockdown of *Tet1* for the following reasons: (1) TET1 has been identified as a hypoxia-sensitive sensor in specific cell types and induces high 5hmC levels in response to hypoxia. We suggested that it may play an important role in IH. (2) TET1 is essential for neurogenesis, and since the hippocampal DG is one of the major regions of adult neurogenesis, we proposed that it is more likely to regulate hippocampal function in the IH context. (3) Studies on the effects of

cognitive function have focused more on TET1 but are highly contradictory, and we aimed to determine the role of TET1 in IH-induced cognitive dysfunction. IF staining showed that TET1 expression was significantly reduced in the nucleus of the DG region. As we predicted, sh*Tet1* treatment resulted in significant improvements in spatial learning and memory, and significant reductions in Wnt Signaling pathway gene demethylation and gene expression. The number of DCX, GFAP and IBA1 positive cells and the levels of multiple inflammatory cytokines tended to be normal, indicating that abnormal neurogenesis and neuroinflammation were limited. In future studies, the effectiveness of TET1 knockdown will be investigated in different subtypes and cell type distributions. In addition, recent studies have shown that intrathecal injection of TET1 specific inhibitor Bobcat 339 can achieve similar therapeutic effects as *Tet1* siRNA on inflammatory pain in mice [95]. It prompted us to consider utilizing this inhibitor in the future to further explore the mechanism of DNA hydroxymethylation in IH-induced cognitive dysfunction. Finally, 5hmC point mutations in Wnt pathway genes were essential to verify that TET1 affects cognitive function by specifically regulating 5hmC.

Conclusions

Our results demonstrated that Wnt pathway gene demethylation was involved in the development of IH-induced cognitive dysfunction in mice by regulating hippocampal neuroinflammation and neurogenesis, which could be reversed by specific knockdown of hippocampal *Tet1*. We hope that our study contributes to the understanding of the underlying mechanisms of cognitive impairment in OSA patients and suggests a potentially effective target for intervention.

Abbreviations

2-OGDD	2-oxoglutarate-dependent dioxygenase
5hmC	5-hydroxymethylcytosine
5mC	5-methylcytosine
BOLD	Blood oxygenation level dependent
CNS	Central nervous system
DDGs	Differentially demethylated genes
DEGs	Differentially expressed genes
DMGs	Differentially methylated genes
fMRI	Functional magnetic resonance imaging
HE	Hematoxylin-eosin
hMeDIP	Hydroxymethylated DNA immunoprecipitation
IF	Immunofluorescence
IHC	Immunohistochemistry
IH	Intermittent hypoxia
MeDIP	Methylated DNA immunoprecipitation
NOR	Novel object recognition
OSA	Obstructive sleep apnoea
PO_2	Partial pressure of oxygen
qRT-PCR	Quantitative real-time qRT-PCR
TET	Ten-eleven translocation

Supplementary Information

The online version contains supplementary material available at https://doi.org/10.1186/s12974-024-03189-2.

Supplementary Material 1
Supplementary Material 2
Supplementary Material 3
Supplementary Material 4
Supplementary Material 5
Supplementary Material 6
Supplementary Material 7
Supplementary Material 8
Supplementary Material 9
Supplementary Material 10
Supplementary Material 11
Supplementary Material 12
Supplementary Material 13
Supplementary Material 14
Supplementary Material 15
Supplementary Material 16
Supplementary Material 17
Supplementary Material 18
Supplementary Material 19
Supplementary Material 20

Acknowledgements

Not applicable.

Author contributions

All authors contributed to the conception and design of the study. KY and JJ conducted most of the experiments, prepared the manuscript and contributed equally. ZX, LF, and YP help analyze data and comment on previous manuscripts. All the authors approved the final draft. Dr. Fei Yang and Dr. Shan wang are the guarantor of this work, and as such, they has full access to all the data in the study and is responsible for the integrity of the data and the accuracy of the data analysis. All authors read and approved the final manuscript.

Funding

This work was supported by grants from National natural science foundation of China (82271193), Public service development and reform pilot project of Beijing Medical Research Institute (BMR2021-3), Capital's Funds for Health Improvement and Research (2022-2-1132), Beijing Hospitals Authority's Ascent Plan (DFL20221102), and Research Foundation of Capital Institute of Pediatrics (LCY-2023-23).

Data availability

Data is provided within the manuscript or supplementary information files.

Declarations

Ethics approval and consent to participate

All experiments were approved by the Animal Care and Use Ethics Committee of the Capital Institute of Pediatrics (DWLL2021016). Anesthesia and euthanasia of animals were consulted with the American Veterinary Medical Association (AVMA) Guidelines for the Euthanasia of Animals (2020).

Consent for publication
Not applicable.

Competing interests
The authors declare no competing interests.

Author details
[1]Children's Hospital Capital Institute of Pediatrics, Chinese Academy of Medical Sciences & Peking Union Medical College, Beijing 100020, China
[2]Graduate School of Peking Union Medical College, Beijing 100730, China
[3]Department of Otolaryngology, Head and Neck Surgery, Children's Hospital Capital Institute of Paediatrics, Beijing 100020, China
[4]Department of Otolaryngology, Head and Neck Surgery, Beijing Children's Hospital, Capital Medical University, National Center for Children's Health, Beijing 100045, China
[5]Beijing Municipal Key Laboratory of Child Development and Nutriomics, Capital Institute of Pediatrics, Beijing 100020, China

Received: 11 April 2024 / Accepted: 29 July 2024
Published online: 21 August 2024

References

1. Benjafield AV, Ayas NT, Eastwood PR, Heinzer R, Ip MSM, Morrell MJ, Nunez CM, Patel SR, Penzel T, Pepin JL, et al. Estimation of the global prevalence and burden of obstructive sleep apnoea: a literature-based analysis. Lancet Respir Med. 2019;7(8):687–98.
2. Patel SR. Obstructive sleep apnea. Ann Intern Med. 2019;171(11):ITC81–96.
3. Hou H, Zhao Y, Yu W, Dong H, Xue X, Ding J, Xing W, Wang W. Association of obstructive sleep apnea with hypertension: a systematic review and meta-analysis. J Glob Health. 2018;8(1):010405.
4. Wang C, Tan J, Miao Y, Zhang Q. Obstructive sleep apnea, prediabetes and progression of type 2 diabetes: a systematic review and meta-analysis. J Diabetes Investig. 2022;13(8):1396–411.
5. Liu X, Ma Y, Ouyang R, Zeng Z, Zhan Z, Lu H, Cui Y, Dai Z, Luo L, He C, et al. The relationship between inflammation and neurocognitive dysfunction in obstructive sleep apnea syndrome. J Neuroinflammation. 2020;17(1):229.
6. da Silva Gusmao Cardoso T, Pompeia S, Miranda MC. Cognitive and behavioral effects of obstructive sleep apnea syndrome in children: a systematic literature review. Sleep Med. 2018;46:46–55.
7. Yu C, Fu Y, Lu Y, Huang Y, Chen F, Wei J, Li L, Ampadu JA, Wang Y, Zheng W, et al. Alterations of brain gray matter volume in children with obstructive sleep apnea. Front Neurol. 2023;14:1107086.
8. Bubu OM, Andrade AG, Umasabor-Bubu OQ, Hogan MM, Turner AD, de Leon MJ, Ogedegbe G, Ayappa I, Jean-Louis GG, Jackson ML, et al. Obstructive sleep apnea, cognition and Alzheimer's disease: a systematic review integrating three decades of multidisciplinary research. Sleep Med Rev. 2020;50:101250.
9. Macey PM, Prasad JP, Ogren JA, Moiyadi AS, Aysola RS, Kumar R, Yan-Go FL, Woo MA, Albert Thomas M, Harper RM. Sex-specific hippocampus volume changes in obstructive sleep apnea. Neuroimage Clin. 2018;20:305–17.
10. Olaithe M, Bucks RS, Hillman DR, Eastwood PR. Cognitive deficits in obstructive sleep apnea: insights from a meta-review and comparison with deficits observed in COPD, Insomnia, and sleep deprivation. Sleep Med Rev. 2018;38:39–49.
11. Bezzi P, Domercq M, Brambilla L, Galli R, Schols D, De Clercq E, Vescovi A, Bagetta G, Kollias G, Meldolesi J, et al. CXCR4-activated astrocyte glutamate release via TNFalpha: amplification by microglia triggers neurotoxicity. Nat Neurosci. 2001;4(7):702–10.
12. Koivunen P, Laukka T. The TET enzymes. Cell Mol Life Sci. 2017;75(8):1339–48.
13. Tahiliani M, Koh KP, Shen Y, Pastor WA, Bandukwala H, Brudno Y, Agarwal S, Iyer LM, Liu DR, Aravind L, et al. Conversion of 5-methylcytosine to 5-hydroxymethylcytosine in mammalian DNA by MLL partner TET1. Science. 2009;324(5929):930–5.
14. Ito S, D'Alessio AC, Taranova OV, Hong K, Sowers LC, Zhang Y. Role of Tet proteins in 5mC to 5hmC conversion, ES-cell self-renewal and inner cell mass specification. Nature. 2010;466(7310):1129–33.
15. Globisch D, Munzel M, Muller M, Michalakis S, Wagner M, Koch S, Bruckl T, Biel M, Carell T. Tissue distribution of 5-hydroxymethylcytosine and search for active demethylation intermediates. PLoS ONE. 2010;5(12):e15367.
16. Szulwach KE, Li X, Li Y, Song CX, Wu H, Dai Q, Irier H, Upadhyay AK, Gearing M, Levey AI, et al. 5-hmC-mediated epigenetic dynamics during postnatal neurodevelopment and aging. Nat Neurosci. 2011;14(12):1607–16.
17. Ellison EM, Abner EL, Lovell MA. Multiregional analysis of global 5-methylcytosine and 5-hydroxymethylcytosine throughout the progression of Alzheimer's disease. J Neurochem. 2017;140(3):383–94.
18. Rudenko A, Dawlaty MM, Seo J, Cheng AW, Meng J, Le T, Faull KF, Jaenisch R, Tsai LH. Tet1 is critical for neuronal activity-regulated gene expression and memory extinction. Neuron. 2013;79(6):1109–22.
19. Antunes C, Da Silva JD, Guerra-Gomes S, Alves ND, Loureiro-Campos E, Pinto L, Marques CJ. Tet3 deletion in adult brain neurons of female mice results in anxiety-like behavior and cognitive impairments. Mol Neurobiol. 2022;59(8):4892–901.
20. Li L, Qiu Y, Miao M, Liu Z, Li W, Zhu Y, Wang Q. Reduction of Tet2 exacerbates early stage Alzheimer's pathology and cognitive impairments in 2×Tg-AD mice. Hum Mol Genet. 2020;29(11):1833–52.
21. Antunes C, Sousa N, Pinto L, Marques CJ. TET enzymes in neurophysiology and brain function. Neurosci Biobehav Rev. 2019;102:337–44.
22. Alaghband Y, Bredy TW, Wood MA. The role of active DNA demethylation and Tet enzyme function in memory formation and cocaine action. Neurosci Lett. 2016;625:40–6.
23. Kwon W, Kim HS, Jeong J, Sung Y, Choi M, Park S, Lee J, Jang S, Kim SH, Lee S, et al. Tet1 overexpression leads to anxiety-like behavior and enhanced fear memories via the activation of calcium-dependent cascade through Egr1 expression in mice. FASEB J. 2018;32(1):390–403.
24. Xu W, Zhang X, Liang F, Cao Y, Li Z, Qu W, Zhang J, Bi Y, Sun C, Zhang J, et al. Tet1 regulates Astrocyte Development and Cognition of mice through modulating GluA1. Front Cell Dev Biol. 2021;9:644375.
25. Kaas GA, Zhong C, Eason DE, Ross DL, Vachhani RV, Ming GL, King JR, Song H, Sweatt JD. TET1 controls CNS 5-methylcytosine hydroxylation, active DNA demethylation, gene transcription, and memory formation. Neuron. 2013;79(6):1086–93.
26. Zhang RR, Cui QY, Murai K, Lim YC, Smith ZD, Jin S, Ye P, Rosa L, Lee YK, Wu HP, et al. Tet1 regulates adult hippocampal neurogenesis and cognition. Cell Stem Cell. 2013;13(2):237–45.
27. Greer CB, Wright J, Weiss JD, Lazarenko RM, Moran SP, Zhu J, Chronister KS, Jin AY, Kennedy AJ, Sweatt JD, et al. Tet1 isoforms differentially regulate gene expression, synaptic transmission, and memory in the mammalian brain. J Neurosci. 2021;41(4):578–93.
28. Thienpont B, Steinbacher J, Zhao H, D'Anna F, Kuchnio A, Ploumakis A, Ghesquiere B, Van Dyck L, Boeckx B, Schoonjans L, et al. Tumour hypoxia causes DNA hypermethylation by reducing TET activity. Nature. 2016;537(7618):63–8.
29. Morin A, Goncalves J, Moog S, Castro-Vega LJ, Job S, Buffet A, Fontenille MJ, Woszczyk J, Gimenez-Roqueplo AP, Letouze E, et al. TET-Mediated hypermethylation primes SDH-Deficient cells for HIF2alpha-Driven mesenchymal transition. Cell Rep. 2020;30(13):4551–e45664557.
30. Mariani CJ, Vasanthakumar A, Madzo J, Yesilkanal A, Bhagat T, Yu Y, Bhattacharyya S, Wenger RH, Cohn SL, Nanduri J, et al. TET1-mediated hydroxymethylation facilitates hypoxic gene induction in neuroblastoma. Cell Rep. 2014;7(5):1343–52.
31. Prasad P, Mittal SA, Chongtham J, Mohanty S, Srivastava T. Hypoxia-mediated epigenetic regulation of stemness in Brain Tumor cells. Stem Cells. 2017;35(6):1468–78.
32. Tsai YP, Chen HF, Chen SY, Cheng WC, Wang HW, Shen ZJ, Song C, Teng SC, He C, Wu KJ. TET1 regulates hypoxia-induced epithelial-mesenchymal transition by acting as a co-activator. Genome Biol. 2014;15(12):513.
33. Ma L, Qi T, Wang S, Hao M, Sakhawat A, Liang T, Zhang L, Cong X, Huang Y. Tet methylcytosine dioxygenase 1 promotes hypoxic gene induction and cell migration in colon cancer. J Cell Physiol. 2019;234(5):6286–97.
34. Coulter JB, O'Driscoll CM, Bressler JP. Hydroquinone increases 5-hydroxymethylcytosine formation through ten eleven translocation 1 (TET1) 5-methylcytosine dioxygenase. J Biol Chem. 2013;288(40):28792–800.
35. Salinas PC. Wnt signaling in the vertebrate central nervous system: from axon guidance to synaptic function. Cold Spring Harb Perspect Biol 2012, 4(2).
36. Arredondo SB, Valenzuela-Bezanilla D, Santibanez SH, Varela-Nallar L. Wnt signaling in the adult hippocampal neurogenic niche. Stem Cells. 2022;40(7):630–40.
37. Marchetti B, Pluchino S. Wnt your brain be inflamed? Yes, it wnt! Trends Mol Med. 2013;19(3):144–56.
38. Jridi I, Canté-Barrett K, Pike-Overzet K, Staal FJT. Inflammation and wnt signaling: target for Immunomodulatory Therapy? Front Cell Dev Biol. 2020;8:615131.

39. Arredondo SB, Valenzuela-Bezanilla D, Mardones MD, Varela-Nallar L. Role of wnt signaling in adult hippocampal neurogenesis in Health and Disease. Front Cell Dev Biol. 2020;8:860.
40. Zhao J, Ikezu TC, Lu W, Macyczko JR, Li Y, Lewis-Tuffin LJ, Martens YA, Ren Y, Zhu Y, Asmann YW, et al. APOE deficiency impacts neural differentiation and cholesterol biosynthesis in human iPSC-derived cerebral organoids. Stem Cell Res Ther. 2023;14(1):214.
41. Xu D, Xu Y, Gao X, Yan M, Zhang C, Wu X, Xia Q, Ge J. Potential value of Interleukin-6 as a diagnostic biomarker in human MDD and the antidepressant effect of its receptor antagonist tocilizumab in lipopolysaccharide-challenged rats. Int Immunopharmacol. 2023;124(Pt B):110903.
42. Khalyfa A, Gozal D, Chan WC, Andrade J, Prasad B. Circulating plasma exosomes in obstructive sleep apnoea and reverse dipping blood pressure. Eur Respir J 2020, 55(1).
43. Wu J, Stefaniak J, Hafner C, Schramel JP, Kaun C, Wojta J, Ullrich R, Tretter VE, Markstaller K, Klein KU. Intermittent hypoxia causes inflammation and Injury to Human Adult Cardiac myocytes. Anesth Analg. 2016;122(2):373–80.
44. Poulain L, Thomas A, Rieusset J, Casteilla L, Levy P, Arnaud C, Dematteis M. Visceral white fat remodelling contributes to intermittent hypoxia-induced atherogenesis. Eur Respir J. 2014;43(2):513–22.
45. Ferrer I, Andrés-Benito P, Carmona M, del Rio JA. Common and specific marks of different tau strains following intra-hippocampal injection of AD, PiD, and GGT inoculum in hTau Transgenic mice. Int J Mol Sci. 2022;23(24):15940.
46. Subramanian A, Tamayo P, Mootha VK, Mukherjee S, Ebert BL, Gillette MA, Paulovich A, Pomeroy SL, Golub TR, Lander ES, et al. Gene set enrichment analysis: a knowledge-based approach for interpreting genome-wide expression profiles. Proc Natl Acad Sci U S A. 2005;102(43):15545–50.
47. Love MI, Huber W, Anders S. Moderated estimation of Fold change and dispersion for RNA-seq data with DESeq2. Genome Biol. 2014;15(12):550.
48. Shannon P, Markiel A, Ozier O, Baliga NS, Wang JT, Ramage D, Amin N, Schwikowski B, Ideker T. Cytoscape: a software environment for integrated models of biomolecular interaction networks. Genome Res. 2003;13(11):2498–504.
49. Zhang X, Lan Y, Xu J, Quan F, Zhao E, Deng C, Luo T, Xu L, Liao G, Yan M, et al. CellMarker: a manually curated resource of cell markers in human and mouse. Nucleic Acids Res. 2019;47(D1):D721–8.
50. Li S, Li L, Li J, Liang X, Song C, Zou Y. miR-203, fine-tunning neuroinflammation by juggling different components of NF-κB signaling. J Neuroinflamm 2022, 19(1).
51. Hu D, Cao Y, He R, Han N, Liu Z, Miao L, Yin J. Schizandrin, an antioxidant lignan from Schisandra chinensis, ameliorates Abeta1-42-induced memory impairment in mice. Oxid Med Cell Longev. 2012;2012:721721.
52. Alexander JF, Seua AV, Arroyo LD, Ray PR, Wangzhou A, Heibeta-Luckemann L, Schedlowski M, Price TJ, Kavelaars A, Heijnen CJ. Nasal administration of mitochondria reverses chemotherapy-induced cognitive deficits. Theranostics. 2021;11(7):3109–30.
53. Zhou L, Chen P, Peng Y, Ouyang R. Role of Oxidative Stress in the Neurocognitive Dysfunction of Obstructive Sleep Apnea Syndrome. *Oxid Med Cell Longev* 2016, 2016:9626831.
54. Lamadema N, Burr S, Brewer AC. Dynamic regulation of epigenetic demethylation by oxygen availability and cellular redox. Free Radic Biol Med. 2019;131:282–98.
55. Matuleviciute R, Cunha PP, Johnson RS, Foskolou IP. Oxygen regulation of TET enzymes. FEBS J. 2021;288(24):7143–61.
56. Burr S, Caldwell A, Chong M, Beretta M, Metcalf S, Hancock M, Arno M, Balu S, Kropf VL, Mistry RK, et al. Oxygen gradients can determine epigenetic asymmetry and cellular differentiation via differential regulation of Tet activity in embryonic stem cells. Nucleic Acids Res. 2018;46(3):1210–26.
57. Joshi K, Liu S, Breslin SJP, Zhang J. Mechanisms that regulate the activities of TET proteins. Cell Mol Life Sci. 2022;79(7):363.
58. Xie J, Xie L, Wei H, Li XJ, Lin L. Dynamic regulation of DNA methylation and brain functions. Biology (Basel) 2023, 12(2).
59. Groves JO, Leslie I, Huang GJ, McHugh SB, Taylor A, Mott R, Munafo M, Bannerman DM, Flint J. Ablating adult neurogenesis in the rat has no effect on spatial processing: evidence from a novel pharmacogenetic model. PLoS Genet. 2013;9(9):e1003718.
60. van der Veer BK, Chen L, Custers C, Athanasouli P, Schroiff M, Cornelis R, Chui JS, Finnell RH, Lluis F, Koh KP. Dual functions of TET1 in germ layer lineage bifurcation distinguished by genomic context and dependence on 5-methylcytosine oxidation. Nucleic Acids Res. 2023;51(11):5469–98.
61. Kim H, Jang WY, Kang MC, Jeong J, Choi M, Sung Y, Park S, Kwon W, Jang S, Kim MO, et al. TET1 contributes to neurogenesis onset time during fetal brain development in mice. Biochem Biophys Res Commun. 2016;471(4):437–43.
62. Yang Q, Cao Q, Yu Y, Lai X, Feng J, Li X, Jiang Y, Sun Y, Zhou ZW, Li X. Epigenetic and transcriptional landscapes during cerebral cortex development in a microcephaly mouse model. J Genet Genomics = Yi Chuan Xue bao. 2024;51(4):419–32.
63. Shuang R, Gao T, Sun Z, Tong Y, Zhao K, Wang H. Tet1/DLL3/Notch1 signal pathway affects hippocampal neurogenesis and regulates depression-like behaviour in mice. Eur J Pharmacol. 2024;968:176417.
64. Gontier G, Iyer M, Shea JM, Bieri G, Wheatley EG, Ramalho-Santos M, Villeda SA. Tet2 rescues Age-Related Regenerative decline and enhances cognitive function in the adult mouse brain. Cell Rep. 2018;22(8):1974–81.
65. Pratt KJB, Shea JM, Remesal-Gomez L, Bieri G, Smith LK, Couthouis J, Chen CP, Roy IJ, Gontier G, Villeda SA. Loss of neuronal Tet2 enhances hippocampal-dependent cognitive function. Cell Rep. 2022;41(6):111612.
66. Antunes C, Da Silva JD, Guerra-Gomes S, Alves ND, Ferreira F, Loureiro-Campos E, Branco MR, Sousa N, Reik W, Pinto L, et al. Tet3 ablation in adult brain neurons increases anxiety-like behavior and regulates cognitive function in mice. Mol Psychiatry. 2021;26(5):1445–57.
67. Yang Q, Wang Y, Feng J, Cao J, Chen B. Intermittent hypoxia from obstructive sleep apnea may cause neuronal impairment and dysfunction in central nervous system: the potential roles played by microglia. Neuropsychiatr Dis Treat. 2013;9:1077–86.
68. Wang H, Wang X, Shen Y, Wang Y, Yang T, Sun J, Liu S. SENP1 modulates chronic intermittent hypoxia-induced inflammation of microglia and neuronal injury by inhibiting TOM1 pathway. Int Immunopharmacol. 2023;119:110230.
69. Li C, Wu Y, Huang MY, Song XJ. Characterization of inflammatory signals in BV-2 microglia in response to Wnt3a. Biomedicines 2023, 11(4).
70. Lazarov O, Hollands C. Hippocampal neurogenesis: learning to remember. Prog Neurobiol. 2016;138–140:1–18.
71. Zhang X, Wei X, Mei Y, Wang D, Wang J, Zhang Y, Li X, Gu Y, Peng G, Sun B. Modulating adult neurogenesis affects synaptic plasticity and cognitive functions in mouse models of Alzheimer's disease. Stem Cell Rep. 2021;16(12):3005–19.
72. Lie D-C, Colamarino SA, Song H-J, Désiré L, Mira H, Consiglio A, Lein ES, Jessberger S, Lansford H, Dearie AR, et al. Wnt signalling regulates adult hippocampal neurogenesis. Nature. 2005;437(7063):1370–5.
73. Arredondo SB, Guerrero FG, Herrera-Soto A, Jensen-Flores J, Bustamante DB, Onate-Ponce A, Henny P, Varas-Godoy M, Inestrosa NC, Varela-Nallar L. Wnt5a promotes differentiation and development of adult-born neurons in the hippocampus by noncanonical wnt signaling. Stem Cells. 2020;38(3):422–36.
74. Schafer ST, Han J, Pena M, von Halbach B, Peters O, Gage J. The wnt adaptor protein ATP6AP2 regulates multiple stages of adult hippocampal neurogenesis. J Neurosci. 2015;35(12):4983–98.
75. Heppt J, Wittmann MT, Schaffner I, Billmann C, Zhang J, Vogt-Weisenhorn D, Prakash N, Wurst W, Taketo MM. Lie DC: beta-catenin signaling modulates the tempo of dendritic growth of adult-born hippocampal neurons. EMBO J. 2020;39(21):e104472.
76. Yoshinaga Y, Kagawa T, Shimizu T, Inoue T, Takada S, Kuratsu J, Taga T. Wnt3a promotes hippocampal neurogenesis by shortening cell cycle duration of neural progenitor cells. Cell Mol Neurobiol. 2010;30(7):1049–58.
77. Kowalczyk A, Filipkowski RK, Rylski M, Wilczynski GM, Konopacki FA, Jaworski J, Ciemerych MA, Sicinski P, Kaczmarek L. The critical role of cyclin D2 in adult neurogenesis. J Cell Biol. 2004;167(2):209–13.
78. Sowers LP, Loo L, Wu Y, Campbell E, Ulrich JD, Wu S, Paemka L, Wassink T, Meyer K, Bing X, et al. Disruption of the non-canonical wnt gene PRICKLE2 leads to autism-like behaviors with evidence for hippocampal synaptic dysfunction. Mol Psychiatry. 2013;18(10):1077–89.
79. Varela-Nallar L, Inestrosa NC. Wnt signaling in the regulation of adult hippocampal neurogenesis. Front Cell Neurosci. 2013;7:100.
80. Martin PM, Stanley RE, Ross AP, Freitas AE, Moyer CE, Brumback AC, Iafrati J, Stapornwongkul KS, Dominguez S, Kivimae S, et al. DIXDC1 contributes to psychiatric susceptibility by regulating dendritic spine and glutamatergic synapse density via GSK3 and Wnt/beta-catenin signaling. Mol Psychiatry. 2018;23(2):467–75.
81. Yu L, Huang L, Zhao Y, Liu S, Zhou R, Yue Y, Sun H, Su X, Liu Q, Li S et al. Atorvastatin promotes Pro/anti-inflammatory Phenotypic Transformation of Microglia via Wnt/β-catenin pathway in hypoxic-ischemic neonatal rats. Mol Neurobiol 2023.

82. Lu Y, Liu M, Guo X, Wang P, Zeng F, Wang H, Tang J, Qin Z, Tao T. miR-26a-5p alleviates CFA-induced chronic inflammatory hyperalgesia through Wnt5a/CaMKII/NFAT signaling in mice. CNS Neurosci Ther. 2023;29(5):1254–71.
83. Yang Y, Zhang Z. Microglia and wnt pathways: prospects for inflammation in Alzheimer's Disease. Front Aging Neurosci. 2020;12:110.
84. Song D, Zhang X, Chen J, Liu X, Xue J, Zhang L, Lan X. Wnt canonical pathway activator TWS119 drives microglial anti-inflammatory activation and facilitates neurological recovery following experimental stroke. J Neuroinflammation. 2019;16(1):256.
85. Yuan S, Shi Y, Guo K, Tang SJ. Nucleoside Reverse transcriptase inhibitors (NRTIs) induce Pathological Pain through Wnt5a-Mediated Neuroinflammation in Aging mice. J Neuroimmune Pharmacology: Official J Soc NeuroImmune Pharmacol. 2018;13(2):230–6.
86. Vallée A. Neuroinflammation in Schizophrenia: the key role of the WNT/β-Catenin pathway. Int J Mol Sci 2022, 23(5).
87. Xiao Y, Guan T, Yang X, Xu J, Zhang J, Qi Q, Teng Z, Dong Y, Gao Y, Li M, et al. Baicalin facilitates remyelination and suppresses neuroinflammation in rats with chronic cerebral hypoperfusion by activating Wnt/β-catenin and inhibiting NF-κB signaling. Behav Brain Res. 2023;442:114301.
88. Abu-Elfotuh K, Abdel-Sattar SA, Abbas AN, Mahran YF, Alshanwani AR, Hamdan AME, Atwa AM, Reda E, Ahmed YM, Zaghlool SS, et al. The protective effect of thymoquinone or/and thymol against monosodium glutamate-induced attention-deficit/hyperactivity disorder (ADHD)-like behavior in rats: modulation of Nrf2/HO-1, TLR4/NF-κB/NLRP3/caspase-1 and Wnt/β-Catenin signaling pathways in rat model. Biomed Pharmacotherapy = Biomedecine Pharmacotherapie. 2022;155:113799.
89. Schneider R, Koop B, Schröter F, Cline J, Ingwersen J, Berndt C, Hartung HP, Aktas O, Prozorovski T. Activation of wnt signaling promotes hippocampal neurogenesis in experimental autoimmune encephalomyelitis. Mol Neurodegeneration. 2016;11(1):53.
90. Dohare P, Cheng B, Ahmed E, Yadala V, Singla P, Thomas S, Kayton R, Ungvari Z, Ballabh P. Glycogen synthase kinase-3β inhibition enhances myelination in preterm newborns with intraventricular hemorrhage, but not recombinant Wnt3A. Neurobiol Dis. 2018;118:22–39.
91. Halleskog C, Mulder J, Dahlström J, Mackie K, Hortobágyi T, Tanila H, Kumar Puli L, Färber K, Harkany T, Schulte G. WNT signaling in activated microglia is proinflammatory. Glia. 2011;59(1):119–31.
92. Halleskog C, Schulte G. Pertussis toxin-sensitive heterotrimeric G(αi/o) proteins mediate WNT/β-catenin and WNT/ERK1/2 signaling in mouse primary microglia stimulated with purified WNT-3A. Cell Signal. 2013;25(4):822–8.
93. Du Y, Yan T, Wu B, He B, Jia Y. Research on the mechanism of antidepressive effect of Suanzaoren Decoction through TLR4/MyD88/NF-κB pathway and Wnt/β-catenin pathway. J Ethnopharmacol. 2024;319(Pt 1):117190.
94. Liddelow SA, Guttenplan KA, Clarke LE, Bennett FC, Bohlen CJ, Schirmer L, Bennett ML, Münch AE, Chung WS, Peterson TC, et al. Neurotoxic reactive astrocytes are induced by activated microglia. Nature. 2017;541(7638):481–7.
95. Yang K, Wei R, Liu Q, Tao Y, Wu Z, Yang L, Wang QH, Wang H, Pan Z. Specific inhibition of TET1 in the spinal dorsal horn alleviates inflammatory pain in mice by regulating synaptic plasticity. Neuropharmacology. 2024;244:109799.

Publisher's Note